City Research Online

City, University of London Institutional Repository

This is the accepted version of the paper.

This version of the publication may differ from the final published version.

Manuscript Number: JCOMP-D-05-00722R1

Title: Numerical simulation of fully nonlinear interaction between steep waves and 2D floating bodies using the QALE-FEM method

Article Type: Regular Article

Section/Category:

Keywords: QALE-FEM; Nonlinear water waves; Spring analogy method; Iterative procedure; 2D floating bodies

Corresponding Author: Dr Qingwei Ma, PhD

Corresponding Author's Institution: City University

First Author: Shiqiang Yan

Order of Authors: Shiqiang Yan; Qingwei Ma, PhD

Manuscript Region of Origin:

Numerical simulation of fully nonlinear interaction between steep waves and 2D floating bodies using the QALE-FEM method

S. Yan and Q.W. Ma

School of Engineering and Mathematical Sciences, City University, London, EC1V 0HB, UK

Abstract

This paper extends the QALE-FEM (Quasi Arbitrary Lagrangian-Eulerian Finite Element Method) based on a fully nonlinear potential theory, which was recently developed by the authors ([1], [2]), to deal with the fully nonlinear interaction between steep waves and 2D floating bodies. In the QALE-FEM method, complex unstructured mesh is generated only once at the beginning of calculation and is moved to conform to the motion of boundaries at other time steps, avoiding the necessity of high cost remeshing. In order to tackle challenges associated with floating bodies, several new numerical techniques are developed in this paper. These include the technique for moving mesh near and on body surfaces, the scheme for estimating the velocities and accelerations of bodies as well as the forces on them, the method for evaluating the fluid velocity on the surface of bodies and the technique for shortening the transient period. Using the developed techniques and methods, various cases associated with the nonlinear interaction between waves and floating bodies are numerically simulated. For some cases, the numerical results are compared with experimental data available in the public domain and good agreement is achieved.

1. Introduction

With operations in the oil and gas industry moving to deeper water, offshore structures are more likely to be exposed to very harsh environments and extremely steep waves and therefore undergo large motions. As a result, there is an increasing interest in numerically simulating nonlinear water waves and their interaction with floating structures. Two classes of theoretical models for cases with finite water depth are in common use for numerical simulations. One is based on general flow theory and the other is based on potential theory. In the first class of models, the Navier-Stokes and continuity equations together with proper boundary conditions are solved; while in the second class, the Laplace equation with fully nonlinear boundary conditions are dealt with. For brevity, the first class of models will be called NS Model and the second called FNPT (representing fully nonlinear potential theory) Model in the paper.

In the community of researchers who use the NS Model, three formulations have been suggested: Eulerian, Lagrangian and arbitrary Lagrangian-Eulerian (ALE) formulations. Various numerical methods, such as finite element, finite volume and finite difference methods have been adopted to

solve the Navier-Stokes and continuity equations together with one of three formulations. However, whichever formulation is used, solving the NS equations is always a time consuming task. As a result, the FNPT Model has been employed in many publications for problems associated with nonlinear water waves and their interaction with structures. In this model, viscosity is ignored. The governing equations are dramatically simplified and therefore need much less computational resources to be solved than in the NS Model. Comparison with experimental data ([3]-[6]) has shown that the results obtained by using this model are accurate enough if breaking waves do not occur and/or if structures involved are large. Therefore, the FNPT Model, instead of the NS Model, should be preferred if a case considered falls in this category.

The problems formulated by FNPT model are usually solved by a time marching procedure suggested by Longuet-Higgins & Cokelet [7]. In this procedure, the key task is to solve the boundary value problem by using an efficient numerical method, such as the boundary element method (BEM) or the finite element method (FEM). The BEM has been attempted by many researchers, such as Vinje & Brevig [8] , Lin, Newman & Yue [9] , Wang, Yao & Tulin [10], Kashiwagi [11], Cao, Schultz & Beck [12], Celebi, Kim & Beck [13], Grilli, Guyenne & Dias [14] and Kim, Celebi & Kim [15]. The FEM has been developed by Wu & Eatock Taylor ([16],[17]) for two dimensional cases and by Ma, Wu & Eatock Taylor ([5],[6]) and Ma [18] for three dimensional cases. All the above publications are concerned with problems either about fixed bodies or those with a prescribed motion. Until now, the publications about the interaction between fully nonlinear waves and free-response bodies are still very limited. Beck & Schultz [19] made nonlinear computation of wave loads and motions of freely rectangular barge in incident waves. Tanizawa [20], Tanizawa & Minami [21] and Tanizawa, Minami & Naito [22] simulated 2D freely barge-type floating body, followed by Koo [23] and Koo & Kim [24]. Kashiwagi & Momoda [25] and Kashiwagi [26] investigated wave-induced motions of 2D complicated-shape floating body. All of them used the BEMs. Recently, Wu & Hu modelled the interaction between waves and a 3D cylindrical FPSO-like structure ([27]) in which the FEM was applied.

Both the BEM and the FEM have been proved efficient but the later require less memory and is therefore computationally more efficient for fully nonlinear wave-body problems, as indicated by Ma, Wu & Eatock Taylor [5] and Wu & Eatock Taylor [16]. A disadvantage of the FEM, however, is that a complex unstructured mesh is necessary for complicated geometries to achieve accurate results, which may need to be regenerated at every time step to follow the motion of waves and bodies. Repeatedly regenerating such a mesh may take a major part of CPU time and so makes the overall simulation very slow. To reduce the CPU time spent on updating the mesh, a simple structured mesh was used in [5]-[6] and [16]-[18]. Wu & Hu [27] recently developed a hybrid mesh for the same purpose but it was restricted only to cylindrical structures without rotational motions because of the limitation of the mesh structure. The problem associated with mesh has become a bottleneck in the development of efficient methods dealing with the interaction between water waves and freely floating bodies. To

overcome the difficulty, Ma and Yan ([1] and [2]) have recently invented a QALE-FEM (Quasi Arbitrary Lagrangian-Eulerian Finite Element Method). The main idea of this method is that the complex unstructured mesh is generated only once at the beginning of calculation and is moved at other time steps to conform to motions of boundaries. This feature allows one to use an unstructured mesh with any degree of complexity without the need of regenerating it at every time step. Ma & Yan [1] compared the QALE-FEM with conventional FEM in terms of computational efficiency and accuracy in the cases with periodic bars on the seabed. They concluded that the QALE-FEM may require less than 15% of the CPU time required by the conventional FEM at the same accuracy level. However, they applied the new method only to cases without floating bodies.

In this paper, the QALE-FEM is extended to deal with problems involving 2D freely floating bodies. In order to tackle the challenges associated with floating bodies, several new numerical techniques are developed. These include a technique for moving the mesh near and on the body surface, a scheme for estimating the velocities and accelerations of bodies as well as the forces on them, a method for evaluating the fluid velocity on the surface of bodies and a technique for shortening the transient period. The last technique is beneficial to investigations of response amplitude operators (RAOs) of floating bodies in waves, which require reaching a steady state (all motions being periodic with roughly constant amplitudes) as soon as possible in order to save CPU time. Using these developed techniques, various cases associated with the nonlinear interaction between waves and floating bodies are numerically simulated. For some cases, the numerical results are compared with experimental data available in the public domain and good agreement is achieved.

2. Mathematical model and numerical method

In this paper, waves are generated by a piston-like wavemaker in a tank as shown in Fig.1. The wavemaker is mounted at the left end and a damping zone with a Sommerfeld condition (see [5] and [18] for details) is applied at the right end of the tank in order to suppress the reflection. A Cartesian coordinate system is used with the *oxy* plane on the mean free surface and with the z-axis being positive upwards. A floating body is placed at *x*=0 initially and moored to the bed or walls of the tank.

2.1. FNPT model for fluid

Similar to the usual formulation for the FNPT Model, the velocity potential (ϕ) satisfies Laplace's equation,

$$\nabla^2 \phi = 0 \tag{1}$$

in fluid domain. On the free surface $z = \zeta(x, y, t)$, the velocity potential satisfies the kinematic and dynamic conditions in the following Lagrangian form,

$$\frac{Dx}{Dt} = \frac{\partial \phi}{\partial x}, \frac{Dy}{Dt} = \frac{\partial \phi}{\partial y}, \frac{Dz}{Dt} = \frac{\partial \phi}{\partial z} \tag{2}$$

$$\frac{D\phi}{Dt} = -gz + \frac{1}{2}|\nabla\phi|^2 \tag{3}$$

where $\dfrac{D}{Dt}$ is the substantial (or total time) derivative following fluid particles and g is the gravitational acceleration. In Eq. (3), the atmospheric pressure has been taken as zero. On all rigid boundaries, such as the wavemaker and the floating body, the velocity potential satisfy

$$\frac{\partial\phi}{\partial n} = \vec{n}\cdot\vec{U}(t) \tag{4}$$

where $\vec{U}(t)$ and $\vec{n}$ are the velocity and the unit normal vector of the rigid boundaries, respectively. The positive direction of the normal vector points to the outside of the fluid domain.
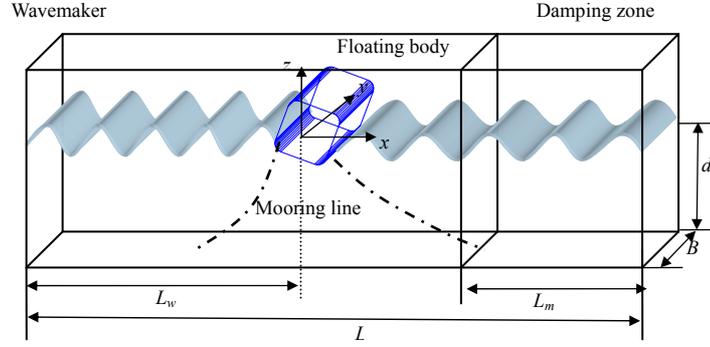

Fig. 1. Sketch of fluid domain

2.2. Motion equations of a floating body

The displacements, velocities and accelerations of a floating body are governed (see, e.g., [18] and [28]) by

$$[M]\dot{\vec{U}}_c = \vec{F} \tag{5a}$$

$$[I]\dot{\vec{\Omega}} + \vec{\Omega}\times[I]\vec{\Omega} = \vec{N} \tag{5b}$$

$$\frac{d\vec{S}}{dt} = \vec{U}_c \tag{6a}$$

$$[B]\frac{d\vec{\theta}}{dt} = \vec{\Omega} \tag{6b}$$

where $\vec{F}$ and $\vec{N}$ are the force and moment acting on the floating body; $\vec{U}_c$ and $\dot{\vec{U}}_c$ the translational velocity and acceleration of its gravitational centre; $\vec{\Omega}$ and $\dot{\vec{\Omega}}$ its angular velocity and acceleration; $\vec{\theta}(\alpha,\beta,\gamma)$ the Euler angles; $\vec{S}$ the translational displacements. In Eq. (5) and (6), $[M]$ and $[I]$ are mass and inertia matrixes, respectively; and $[B]$ is the matrix formed by Euler angles and defined as,

$$[B] = \begin{bmatrix} \cos\beta\cos\gamma & \sin\gamma & 0 \\ -\cos\beta\sin\gamma & \cos\gamma & 0 \\ \sin\beta & 0 & 1 \end{bmatrix} \tag{7}$$

In 2D cases, $\vec{\Omega} \times [I]\vec{\Omega} = 0$, $\alpha = 0, \gamma = 0$, Eqs (5b) and (6b) can be rewritten as

$$[I]\dot{\vec{\Omega}} = \vec{N} \tag{8}$$

$$\frac{d\vec{\theta}}{dt} = \vec{\Omega} \tag{9}$$

Once $\vec{U}_c$ and $\vec{\Omega}$ are known, the velocity at a point on the body is determined by

$$\vec{U} = \vec{U}_c + \vec{r}_b \times \vec{\Omega} \tag{10}$$

where r_b is the position vector relative to the gravitational centre.

2.3. Force calculation

The force ($\vec{F}$) and moment ($\vec{N}$) acting on a body in Eqs. (5) and (6) can be evaluated by,

$$\vec{F} = -\rho \iint_{S_b} \left(\frac{\partial\phi}{\partial t} + \frac{1}{2}|\nabla\phi|^2 + gz \right) \vec{n}\,ds + \vec{f}_m \tag{11}$$

$$\vec{N} = -\rho \iint_{S_b} \left(\frac{\partial\phi}{\partial t} + \frac{1}{2}|\nabla\phi|^2 + gz \right) \vec{r}_b \times \vec{n}\,ds + \vec{N}_m \tag{12}$$

where S_b denotes the wetted body surface. $\vec{f}_m$ and $\vec{N}_m$ are forces and moments due to mooring lines, respectively. Because this paper focuses on the wave-body interaction, the mooring lines are approximated by using linear springs, i.e.,

$$\vec{f}_m = k_m \vec{S}_m \tag{13a}$$

$$\vec{N}_m = \vec{r}_m \times \vec{f}_m \tag{13b}$$

in which k_m is the spring stiffness, $\vec{S}_m$ is the displacement of the mooring point, $\vec{r}_m$ is the position vector of the mooring point relative to the gravitational centre.

As can be seen, the time derivative of the velocity potential ($\partial\phi/\partial t$) is required and is critical for accurately calculating forces and moments. A simplest way to calculate $\partial\phi/\partial t$ is to use a backward finite difference scheme:

$$\left(\frac{\partial\phi}{\partial t} \right)^n = \frac{\phi^n - \phi^{n-1}}{\Delta t} \tag{14}$$

where Δt is the time step and the superscript n denotes n^{th} time step. As is well known, however, the scheme may suffer from a problem of the saw-tooth instabilities ([29]). An alternative approach is to

5

find $\partial\phi/\partial t$ by solving a similar boundary value problem to that for ϕ defined in Eqs. (1)-(4) (see, for example,[5]-[6], [16]-[18]). The boundary value problem for $\partial\phi/\partial t$ is defined by,

$$\nabla^2\left(\frac{\partial\phi}{\partial t}\right) = 0 \tag{15}$$

in the fluid domain. On the free surface $z = \zeta(x, y, t)$, it is given by

$$\frac{\partial\phi}{\partial t} = -g\zeta - \frac{1}{2}|\nabla\phi|^2 \tag{16}$$

On all rigid boundaries, it satisfies

$$\frac{\partial}{\partial n}\left(\frac{\partial\phi}{\partial t}\right) = [\vec{U}_c + \vec{\Omega}\times\vec{r}_b]\cdot\vec{n} - \vec{U}_c\cdot\frac{\partial\nabla\phi}{\partial n} + \vec{\Omega}\cdot\frac{\partial}{\partial\vec{n}}[\vec{r}_b\times(\vec{U}_c - \nabla\phi)]. \tag{17}$$

It should be noted here that there is a difficult with solving Eqs. (15) to (17). As can be seen from Eq. (17), the accelerations $\dot{\vec{U}}_c$ and $\dot{\vec{\Omega}}$ should be known when solving the boundary value problem for $\partial\phi/\partial t$. However, in cases involving a free-response floating body, they are evaluated by Eqs. (5) and (6), which depends on the force and moment given in Eqs. (11) and (12). In turn, to find the force and moment, one needs $\partial\phi/\partial t$. The scheme to overcome this difficulty will be detailed in Section 5 below.

2.4. FEM formulation

The full details about the FEM formulation have been discussed in our previous publications, for example [1], [5] and [18]. They will not be repeated here. Only summary of the formulation is given below.

The problem described by Eqs. (1) to (4) will be solved by using a time step marching procedure. At each time step, the free surface and the potential values on it as well as velocities on all rigid boundaries are known. Thus, the boundary condition for the potential on the free surface can be replaced by a Dirichlet condition:

$$\phi = f_p \tag{18}$$

where f_p is the potential values on the free surface, which can be estimated by using Eq. (3) and a time integration scheme with second order accuracy. Therefore, the unknown velocity potential in the fluid domain can be found by solving a mixed boundary value problem which is defined by Eqs. (1), (4) and (18). To do so, the fluid domain is discretised into a set of small tetrahedral elements and the velocity potential is expressed in terms of a linear shape function, $N_J(x, y, z)$:

$$\phi = \sum_J \phi_J N_J(x, y, z) \tag{19}$$

where ϕ_J is the velocity potential at Node J. Using the Galerkin method, the Laplace equation and the

boundary conditions are discretised as follows,

$$\iiint_\forall \nabla N_I \cdot \sum_{\substack{J \\ J \notin S_P}} \phi_J \nabla N_J d\forall = \iint_{S_n} N_I f_n dS - \iiint_\forall \nabla N_I \cdot \sum_{\substack{J \\ J \in S_P}} (f_p)_J \nabla N_J d\forall \tag{20}$$

where S_P represents the Dirichlet boundary on which the velocity potential f_p is known and S_n represents the Numann boundary on which the normal derivative of the velocity potential f_n is known. Eq. (20) can further be written in the matrix form:

$$[A]\{\phi\} = \{B\} \tag{21}$$

where

$$\{\phi\} = [\phi_1, \phi_2, \phi_3, \ldots, \phi_I, \ldots]^T \qquad (I \notin S_P) \tag{22a}$$

$$A_{IJ} = \iiint_\forall \nabla N_I \cdot \nabla N_J d\forall \qquad (I \notin S_P, J \notin S_P) \tag{22b}$$

$$B_I = \iint_{S_n} N_I f_n dS - \iiint_\forall \nabla N_I \cdot \sum_{J \in S_P} (f_p)_J \nabla N_J d\forall \qquad (I \notin S_P) \tag{22c}$$

The algebraic Eq. (21) is solved by using a conjugate gradient iterative method with SSOR pre-conditioner and optimised parameters [18]. The problem about $\partial \phi / \partial t$ described in Eqs. (15) to (17) is also solved by using the above method with ϕ and the boundary conditions for it are replaced by $\partial \phi / \partial t$ and corresponding boundary conditions for $\partial \phi / \partial t$.

3. Summary of QALE-FEM method

As indicated in the Introduction, the QALE-FEM developed in [1] will be extended in this paper to deal with problems with 2D floating bodies. In this section, the key elements of the QALE-FEM in [1] are summarised before presenting new developments of this paper.

3.1. Scheme for moving mesh

The main idea of the QALE-FEM is that the complex unstructured mesh is generated only once at the beginning of calculation and is moved at other time steps to conform to the motion of boundaries. Obviously, the technique for moving the mesh is crucial in this method to achieve high robustness and high efficiency. For this purpose, a novel methodology is suggested and adopted, in which interior nodes and boundary nodes are considered separately; the nodes on the free surface and on rigid boundaries are considered separately; nodes on the free surface are split into two groups: those on waterlines and those not on waterlines (inner-free-surface nodes); and different methods are employed for moving different nodes.

To move the interior nodes which do not lie on boundaries, a spring analogy method is used. In this method, nodes are considered to be connected by springs and the whole mesh is then deformed like a spring system. Specifically, the nodal displacement is determined by

$$\Delta \vec{r}_i = \sum_{j=1}^{N_i} k_{ij} \Delta \vec{r}_j \Bigg/ \sum_{j=1}^{N_i} k_{ij} \qquad (23)$$

where $\Delta \vec{r}_i$ is the displacement at Node I; k_{ij} is the spring stiffness and N_i is the number of nodes that are connected to Node I. For problems about nonlinear water waves, it is crucial to maintain the quality (good element shapes and reasonable node distribution) of mesh near the free surface. To do so, the spring stiffness in the QALE-FEM is suggested as

$$k_{ij} = \frac{1}{l_{ij}^2} e^{\gamma \left[1 + (z_i + z_j)/2d \right]} \qquad (24)$$

where k_{ij} is the spring stiffness, l_{ij} is the distance between Nodes I and J; z_i and z_j are the vertical coordinates of Nodes I and J; d is the water depth; and γ is an coefficient that should be assigned a larger value if the springs are required to be stiffer at the free surface. The spring analogy method is also used for moving nodes on rigid boundaries.

The positions of nodes on the free surface are determined by physical boundary conditions, i.e., following the fluid particles at most time steps. The nodes moved in this way may become too close to or too far from each other. To prevent this from happening, these nodes are relocated at a certain frequency, e.g. every 40 time steps. When doing so, the nodes on the waterlines is re-distributed by adopting a principle for a self-adaptive mesh, i.e., the weighted arc-segment lengths satisfies

$$\varpi_i \Delta s_i = C_s \qquad (25)$$

where ϖ is a weighted function, Δs_i the arc-segment length between two successive nodes and C_s a constant. In order to relocate the inner-free-surface nodes, they are first moved using the spring analogy system in the projected plane of the free surface, resulting in new coordinates x and y; and then the elevations of the free surface corresponding to the new coordinates are evaluated by an interpolating method. In order to take into account of the local gradient of the free surface, however, the spring stiffness for moving the nodes in x- and y- directions is determined, respectively, by:

$$k_{ij}^{(x)} = \frac{1}{l_{ij}^2} \sqrt{1 + \left(\frac{\partial \zeta}{\partial x} \right)^2} \quad \text{and} \quad k_{ij}^{(y)} = \frac{1}{l_{ij}^2} \sqrt{1 + \left(\frac{\partial \zeta}{\partial y} \right)^2} \ . \qquad (26)$$

where $k_{ij}^{(x)}$ and $k_{ij}^{(y)}$ are the spring stiffness; $\dfrac{\partial \zeta}{\partial x}$ and $\dfrac{\partial \zeta}{\partial y}$ the local slopes of the free surface in the x- and y-directions, respectively. The numerical tests in [1] have shown that the scheme for moving mesh is very robust and very efficient.

3.2. Calculation of fluid velocities on the free surface

The mesh used in the QALE-FEM is arbitrarily unstructured and moving during the calculation. An effective method to calculate the fluid velocity on the free surface under this condition is developed in [1]. In this method, the velocity at a node I with neighbours J_k (k=1,2,3, ……, m) on the

free surface is split into normal and tangential components. To estimate the normal component of the velocity, two points on the normal line at Node *I* are selected firstly and the velocity potentials at these two points are then approximated by using a moving least square method. The normal component ($\vec{v}_n$) of the velocity is determined by a three-point finite difference scheme:

$$\vec{v}_n = \left[\frac{2}{3h_{I1}} \left(\frac{2h_{I1} + h_{I2}}{h_{I1} + h_{I2}} + \frac{1}{2} \right) \phi_I - \left(\frac{2}{3h_{I2}} + \frac{1}{h_{I1}} \right) \phi_{I1} + \frac{2}{3h_{I2}} \left(\frac{h_{I1}}{h_{I1} + h_{I2}} \right) \phi_{I2} \right] \vec{n} \,. \tag{27}$$

where *I1* and *I2* represent the two points selected; h_{I1} and h_{I2} are the distances between *I* and *I1* and between *I1* and *I2*, respectively; and ϕ_I, ϕ_{I1} and ϕ_{I2} denote the velocity potentials at the node and the two points; the later two, ϕ_{I1} and ϕ_{I2}, are found by a moving least square method. After the normal component of the velocity is determined, the tangential components of the velocity is calculated using a least square method based on the following equation

$$\vec{v}_{\tau_x} \cdot \vec{l}_{IJ_k} + \vec{v}_{\tau_y} \cdot \vec{l}_{IJ_k} = \vec{l}_{IJ_k} \cdot \nabla\phi - \vec{v}_n \cdot \vec{l}_{IJ_k} \quad (\, k=1,2,3, \ldots\ldots, m) \tag{28}$$

where $\vec{l}_{IJ_k}$ is the unit vector from Node *I* to Node J_k; $\vec{v}_{\tau_x}$ and $\vec{v}_{\tau_y}$ represent the velocity components in $\vec{\tau}_x$ and $\vec{\tau}_y$ directions, respectively. These directions are determined by $\vec{\tau}_x \perp \vec{n}$, $\vec{\tau}_x /\!/ \vec{e}_x$, $\vec{\tau}_y \perp \vec{n}$ and $\vec{\tau}_y /\!/ \vec{e}_y$, where $\vec{e}_x$ and $\vec{e}_y$ are the unit vectors in the *x*- and *y*-directions, respectively.

4. Mesh moving scheme associated with floating bodies

The new developments of this paper for dealing with problems with a 2D floating body will be presented in the next three sections. They mainly contain three aspects: 1) mesh moving when a floating body is involved; 2) calculation of fluid velocities on the surface of the floating body and 3) estimation of velocities of the floating body and forces on it. The first aspect is presented in this section.

The basic strategy and principle to move the mesh are similar to that for the problem without floating bodies as summarised above. Nevertheless, special considerations must be devoted to the mesh near the body and on its surface, which is discussed in the following two subsections.

4.1. Moving interior nodes

Interior nodes are moved by the analogy spring method, similar to that for problems without floating bodies as outlined above. However, with a floating bode involved, the mesh must preserve a reasonable element shape and node distribution not only in the vicinity of the free surface but also in the region close to the floating body, i.e. the near-body-region, as illustrated in Fig.2. To achieve this, the springs near both the free and body surfaces are chosen to be stiffer than those in other areas, that is, Eq. (24) is replaced by

$$k_{ij} = \frac{1}{l_{ij}^2} e^{\gamma_f \left[1 + (z_i + z_j)/2d \right]} e^{\gamma_b (\hat{w}_i + \hat{w}_j / 2)} \tag{29}$$

where γ_f is the same as γ in Eq. (24); γ_b plays the same role as γ_f but is used to adjust the spring stiffness near the body surface. The two coefficients may be different but in this paper they are taken to be the same values, i.e., $\gamma_f = \gamma_b = 1.7$. In Eq. (29), $\hat{w}$ is a weight function and is determined by,

$$\hat{w} = \begin{cases} 0 & d_f > D_f \\ 1 - d_f / D_f & d_f \leq D_f \end{cases} \tag{30a}$$

where d_f is the minimum distance from the node concerned to the body surface as shown in Fig. 2; D_f is the distance between the body surface and the boundary of the near-body-region and is defined as,

$$D_f = \varepsilon d_{c\max} \tag{30b}$$

where $d_{c\max}$ is the maximum distance from the gravitational centre to the wetted body surface and depends on the relative position of the floating body to the free surface. Numerical tests show that ε = 1.5 is suitable. It can be seen from Eq. (29) and (30) that the spring stiffness outside the near-body-region is the same as that for problem without a floating body.
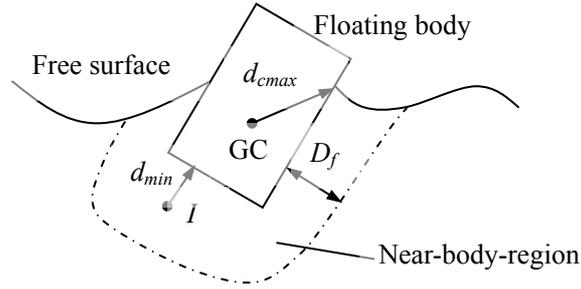

Fig. 2 Region near floating body (GC: Gravitational centre)

4.2. Moving nodes on body surfaces

The wetted body surface is time-dependent in the problems considered here. In order to conform to the change in the wetted body surface, the nodes on the surface must also be moved at each time step. The principle for doing so is similar to that for moving the nodes on the free surface, i.e., splitting the nodes into two groups: nodes on the waterline and nodes lying on the body surface but not on the waterline, the later called inner-body-surface nodes. For 2D problems, there are only two nodes on the waterline. They are moved by using the tangential velocity of the fluid relative to the body surface. The inner-body-surface nodes may appear to be moved by the same approach for moving inner-free-surface nodes, i.e., projecting the nodes onto a horizontal plane, moving the nodes in it by using the spring analogy method and then finding the new positions of nodes on the body surface by interpolation. This approach is obviously subjected to a condition that the surface must have only one

intersecting point with any vertical line; in other words, it can be expressed by a single-valued function. However, this is not always true for floating body surfaces, particularly when they undergo angular motions, such as roll and/or pitch. Therefore, one can not actually use the same approach as for moving the inner-body-surface nodes. A new approach is developed here. In this new approach, the spring analogy method is applied in a local coordinate system formed by the local tangential and normal lines. In this local coordinate system, the body surface is single–valued; i.e., there is only one intersecting point between the body surface and a line parallel to the local normal line (and, of course, perpendicular to the local tangential line). A node, e.g., i, is first moved along the tangential line by

$$\Delta \vec{r}_{i\tau} = \sum_{j=1}^{N_i} k_{ij} \Delta \vec{r} \cdot \vec{\tau}_i \left/ \sum_{j=1}^{N_i} k_{ij} \right. \tag{31}$$

where $\vec{\tau}_i$ is the tangential direction at node i. After that, the new position of the nodes on the body surface is found by interpolation in the local coordinate system. The spring stiffness in Eq. (31) is taken as $k_{ij} = 1/l_{ij}^2$.

It should be noted that at a sharp corner, there will be no unique tangential and normal lines and so the above approach fails. The remedy for overcoming the difficulty is to prescribe a node at the corner or to smooth the corner. Either way works well and gives similar results based on our numerical tests. It should also be noted that the new approach described in this sub-section may be employed to move inner-free-surface nodes when overturning waves are involved, though they are not considered in the paper.

5. Calculations of fluid velocity on the surface of the floating body

The velocity potential on the floating body surface always satisfies Eq. (4) and so the normal components of fluid velocity on the body surface can be determined by

$$\vec{v}_n = \vec{n} \cdot \vec{U}(t) = \vec{n} \cdot (\vec{U}_c + \vec{\Omega} \times \vec{r}_b) \tag{32}$$

Eq. (28) is then used to estimate the tangential component of fluid velocity on the body surface. In 2D cases, it is similar to a central difference scheme at the inner-body-surface nodes. However, at the nodes on the waterline, it becomes similar to a backward scheme due to unsymmetrical distribution of nodes around the waterline and so becomes less accurate than at the inner-body-surface nodes. As an alternative, the tangential velocity at waterline nodes is estimated by using a three-point method similar to Eq. (27). The normal line required by Eq. (27) is taken as a line (τ_w) tangent to the body surface, as shown in Fig. 3. The three points contain the node on the waterline and other two points on the line τ_w. The velocity potentials at the two points (marked as empty circles in Fig. 3) are found using the same method as that for $I1$ and $I2$ in Eq. (27).
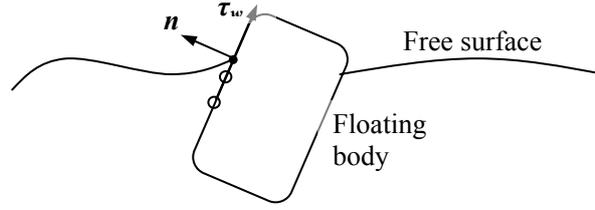
Fig. 3 Definition of tangential and normal directions at a node on the waterline

6. Calculation of forces on and velocities of the floating body

In this paper, $\partial \phi / \partial t$, involved in Eqs. (11) and (12) for estimating the forces on floating bodies, is calculated by solving a boundary value problem defined in Eqs. (15)-(17). As discussed in Section 2.3, there is difficulty with doing so due to the nonlinear coupling between the body and wave motions. In order to tackle this difficulty, four types of methods have been suggested in the literature, i.e. the indirect method, the mode-decomposition method, the Dalen & Tanizawa's method and the iterative method. The indirect method was developed by Wu & Eatock Taylor [16] and followed by Kashiwagi & Momoda [25] and Kashiwagi [26], Wu & Hu [27]. In this method, some auxiliary functions were introduced to decouple the mutual dependence between the force and the acceleration of the body. The mode-decomposition method was suggested by Vingi & Brevig [8] and adopted by Koo [23] and Koo & Kim [24]. In this approach, the body acceleration is decomposed into several modes (4 modes in 2D cases or 7 modes in 3D cases, respectively). Every mode is found by solving a boundary value problem similar to that for the velocity potential but under different boundary conditions. Using these modes and the body-motion equations, the body acceleration is determined. Both these methods have to solve 4 or 7 extra Laplace equations under different boundary conditions. The CPU time, therefore, may be considerably increased if employing an iterative procedure rather than a direct solution scheme (such as Gauss Elimination) which is unlikely to be suitable for solving the corresponding linear algebraic system containing a very large number of unknowns. In the method proposed by Dalen [30] and Tanizawa in [20] and [31], the body accelerations in Eq. (17) are implicitly substituted by the Bernoulli's equations and thus the velocity potential and its time derivative are solved without the need of calculating accelerations of the floating bodies. However, this method requires one to form a special matrix for $\partial \phi / \partial t$ which is different from the one for the velocity potential and whose properties have not been sufficiently studied. This is likely to increase the difficulty for numerically solving the algebraic equations associated with $\partial \phi / \partial t$ and also needs more CPU time for generating the special matrix. That would be the main reason for this method not to be commonly used. Cao, Beck. & Schultz [19] suggested an iterative method to calculate the force and acceleration at each time step; in this way, the need to solve extra equations in the first two methods and the problem with the third method is eliminated.

For the purpose of time marching, a standard explicit 4th-order Runge-Kutta scheme is generally

used to update the velocity of the floating body, which requires three sub-step calculations at one time step forward. In each sub-step, the geometry of the computational domain may or may not be updated. If it is not updated, it is called a frozen coefficient method; if it is update, it is called a fully updated method. The CPU time spent on updating in the fully updated method is roughly equal to 4 times that in the frozen coefficient method. However, the frozen coefficient may not lead to stable and reasonable results for problems with large motions of floating bodies, as indicated by Koo & Kim [24].

The body velocity is estimated from the acceleration at previous time steps (or sub-steps) in all the above methods; i.e., the corresponding procedure is explicit. The explicit procedure may be satisfactory if time steps and so changes in the velocity and acceleration in one step are sufficiently small; otherwise, it may degrade the accuracy and even lead to instability.

In this paper, an improved iterative procedure, called Iterative Semi Implicit Time Integration Method for Floating Bodies (ISITIMFB), is developed, which takes some advantages and overcome some disadvantages of other methods. This method features by (a) using the acceleration in the current step to estimate the body velocity, i.e., it is implicit, distinguishing it from all other methods discussed above; (b) not requiring sub-step calculations, different from the fully updated Runge-Kutta method; (c) eliminating the necessity of solving the extra equations as in the indirect method and the mode-decomposition method and the need to generate a special matrix in the Dalen & Tanizawa's method, getting rid of the main disadvantages of all three; (d) not updating the positions of the free surface and the floating body during the iteration to find the acceleration and force, saving the CPU time spent not only on this but also on forming the new coefficient matrix. The details of the method are described as follows.

Suppose that all calculations until $t=t_{n-1}$ have been finished and so the velocity potential and its time derivative on the free surface, the positions of all boundaries including the free surface and the body surface have been obtained through updating. To find the fluid and body velocities at time t_n, the following procedure is used.

1) Predict the body acceleration $\vec{A}^{n(0)}$ at time t_n by curve fitting of accelerations at previous time steps using a least square method [34] and estimate the corresponding body velocity by using the Adams-Moulton method [35] as following,

$$\vec{U}_b^{n(0)} = \vec{U}_b^{n-1} + \frac{\Delta t}{12}(5\vec{A}_b^{n(0)} + 8\vec{A}_b^{n-1} - \vec{A}_b^{n-2})$$ (33)

where $\vec{A}^{n(0)}$ and $\vec{U}_b^{n(0)}$ represent the predicted values of translational or angular body accelerations and velocities, respectively, at the current time step, which are used as the initial values of iteration.

2) Solve the boundary value problem for ϕ using $\vec{U}_b^{n(0)}$ in Eq. (4) for the boundary condition on the body surface.

3) Calculate the fluid velocity and the time derivative of the velocity potential on the free

surface.

4) Calculate the fluid velocity $\vec{V}_b^{n(0)}$ on the body surface.

5) Using the following loop to find the acceleration of and forces on the body:

(a) Solve the boundary value problem for $\left(\dfrac{\partial \phi}{\partial t}\right)^{n(k)}$ using $\vec{A}^{n(k-1)}, \vec{U}_b^{n(k-1)}$ and $V_b^{n(k-1)}$

in its boundary condition on the body surface (Eq. (17)), where the subscript $n(k-1)$ represent the variables at time t_n but at k-th iteration ($k=1,2,3\ldots\ldots$);

(b) Calculate the forces or moments $\vec{F}^{n(k)}$ and so the acceleration

$$\vec{A}_b^{\,n(k)} = [M]^{-1}\left[\alpha^n \vec{F}^{n(k)} + (1-\alpha^n)\vec{F}^{n(k-1)}\right]; \tag{34}$$

in which mass matrix $[M]$ should be changed to the moment matrix of the mass $[I]$, (Eq. (8)), if the annular acceleration and moment are concerned;

(c) Estimate the new body velocity using the similar method to Eq. (33)

$$\vec{U}_b^{n(k)} = \vec{U}_b^{n-1} + \frac{\Delta t}{12}(5\vec{A}_b^{n(k)} + 8\vec{A}_b^{n-1} - \vec{A}_b^{n-2}); \tag{35}$$

(d) Solve the boundary value problem for ϕ using $\vec{U}_b^{n(k)}$ in Eq. (4) for the boundary condition on the body surface;

(e) Calculate the new fluid velocity $\vec{V}_b^{n(k)}$ on the body surface;

(f) Check if the relative error of accelerations (or forces) is small enough; if not, go to a); otherwise go to 6).

6) Update the position of the body using the final body velocity and acceleration in the above loop by using the 3rd order Taylor expansion,

$$\vec{S}_b^{\,n+1} = \vec{S}_b^{\,n} + \vec{U}^{n(u)}\Delta t + \frac{\Delta t^2}{2}\vec{U}^{n(u)} + \frac{\Delta t^3}{6}\frac{d\vec{U}^{n(u)}}{dt} \tag{36}$$

where $\vec{S}_b^{\,n+1}$ is the translational or annular displacement of the body to be used for the calculation of the next time step; $\vec{U}^{n(u)}$ and $\vec{U}^{n(u)}$ represent the final values of body velocities and accelerations (translational or annular) in the above loop, respectively; and

$\dfrac{d\vec{U}^{n(u)}}{dt}$ is calculated by using the finite difference scheme $\dfrac{d\vec{U}^{n(u)}}{dt} = \left(\vec{U}^{n(u)} - \vec{U}^{n-1(u)}\right)/\Delta t$.

7) Calculate the fluid velocity on the free surface using the final velocity potential in the above loop.

8) Update the time derivative of the velocity potential on and the positions of the free surface using the same method as in [5] and [18].

9) Go to next time step.

As can be seen, an under-relaxation in Eq. (34) is employed in the iterative loop from (a) to (f) to improve the convergent efficiency. The value of α^n is determined by

$$\alpha^n = \frac{A_b^{n-1(u)} - A_b^{n-1(0)}}{A_b^{n-1(1)} - A_b^{n-1(0)}} \tag{37}$$

where $A_b^{n-1(u)}$ is the final value of the acceleration in the iteration at the previous step. This expression is proposed by considering the fact that if one had known α^{n-1}, the solution for $A_b^{n-1(u)}$ would have been found in one iteration through (a) to (f) and by assuming that $\alpha^n \approx \alpha^{n-1}$.

The efficiency of the iterative procedure is signified by the iterative counter (or the number of iterations) in the above loop - the smaller iterative counter the more efficient. One may understand that the iterative counter for a specified accuracy depends on the quality of the predicted velocity in Eq. (33) and three values of the acceleration in Eq. (35). The better prediction of the velocity and the closer values of the acceleration should lead to the smaller number of iterations. The quality of the predicted velocity and the values of the acceleration are in turn determined by the time step, the amplitude of the body motions and the natural frequency of the system. It is expected that the velocity is better predicted and three values of the acceleration becomes closer and hence the iterations is fewer if the time step and the amplitude are smaller and/or if the natural period is larger. For the given wave and the shape of the body, the largest motion amplitude is related to the natural period. Therefore, the two most important factors affecting the iterative counter may be the time step and the natural period. Their effects are to be investigated in Section 7.2.2.

This iterative procedure is distinguished from one in [19] by three aspects. (1): The velocity potential (and so the fluid velocity) is obtained in [19] by assuming that the body velocity in Eq. (4) is estimated using the acceleration at the previous time step and thus the boundary value problem for ϕ is solved only once, i.e. without Step (d), in the above loop. Therefore the procedure in [19] is actually an explicit method as implied above. (2): The relaxation scheme in Eq. (34) and the corresponding relaxation coefficient in Eq. (37) are employed in this paper while it is not clear whether any relaxation is adopted in [19]. (3): The body velocity used in Eq. (4) is continually updated here by employing the scheme as given in Eqs. (33) and (35), while it needs to be evaluated only once in [19].

It has been pointed out that the body and free surface positions are not updated in the iteration loop in the above procedure. That is why this method is classified as 'Semi Implicit'. In this aspect, it is similar to the frozen coefficient method. However, this procedure has not been found to suffer the instability problem associated with the frozen coefficient method; instead, it has been found to share the similar stable behaviour with the full updated Runge-Kutta method. Numerical demonstration of this will be given below.

7. Validations and discussions

In this section, the QALE-FEM method is validated by comparing its numerical predictions with analytical solutions and published results from other papers. Unless mentioned otherwise, the parameters with a length scale are nondimensionalised by the water depth d; and other parameters, including the time and frequency, by

$$t \rightarrow \tau\sqrt{d/g} \text{ and } \omega \rightarrow \omega\sqrt{g/d} .$$

7.1. Forced-motion bodies

Although the main aim of this paper is to simulate cases involving 2D free-response floating bodies, the case for a 2D body in forced motions is investigated in the first stage in order to validate the force calculation, in which the iteration loop discussed in the previous section becomes unnecessary since the body acceleration does not need to be found. The body in these cases is formed with a circular cylinder as the submerged part and vertical walls above it, as shown in Fig.4 (a). The dimensionless radius of the cylinder ($\overline{R}_b$) is 0.25. The initial mesh around the body is similar to that in Fig. 4(b) but much finer.

(a) floating body   (b) initial mesh near the body
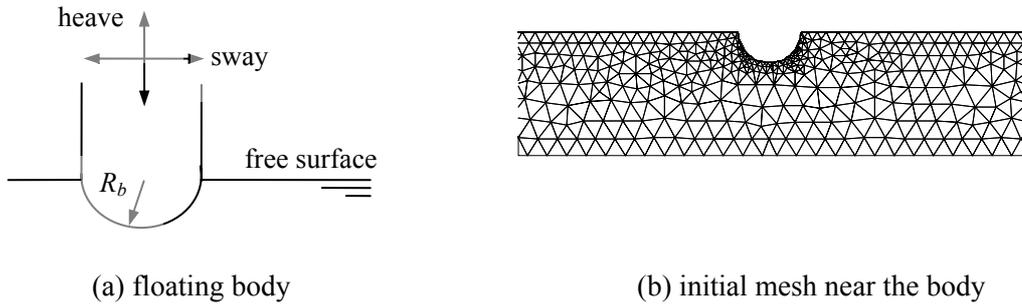
Fig.4 Sketch of body motions and illustration of initial mesh

The displacement (η) of the body is specified by

$$\eta(\tau) = a_b \sin(\omega_b \tau) \tag{38}$$

where a_b and ω_b are the amplitude and circular frequency of the motion, respectively. The velocity corresponding to Eq. (38) is $\vec{U}_c(\tau) = a_b \omega_b \cos(\omega_b \tau)$. This implies that the floating body suddenly gain a finite value of velocity from rest, which is not only practically impossible but also can result in a numerical difficult ([32]-[33]). To avoid it, the velocity $\vec{U}_c$ is ramped as in [33] and given by

$$\vec{U}_c(\tau) = a_b \omega_b \cos(\omega_b \tau)(1 - e^{\beta\tau}) \tag{39a}$$

$$\beta = -\chi\omega_b / 2\pi \tag{39b}$$

where χ is a coefficient. The larger the value of χ, the shorter the time is, during which the effects of

the ramp function persist, though the value does not affect the final results. In this paper, $\chi = 5$ is used.

(a) forced sway (b) forced heave
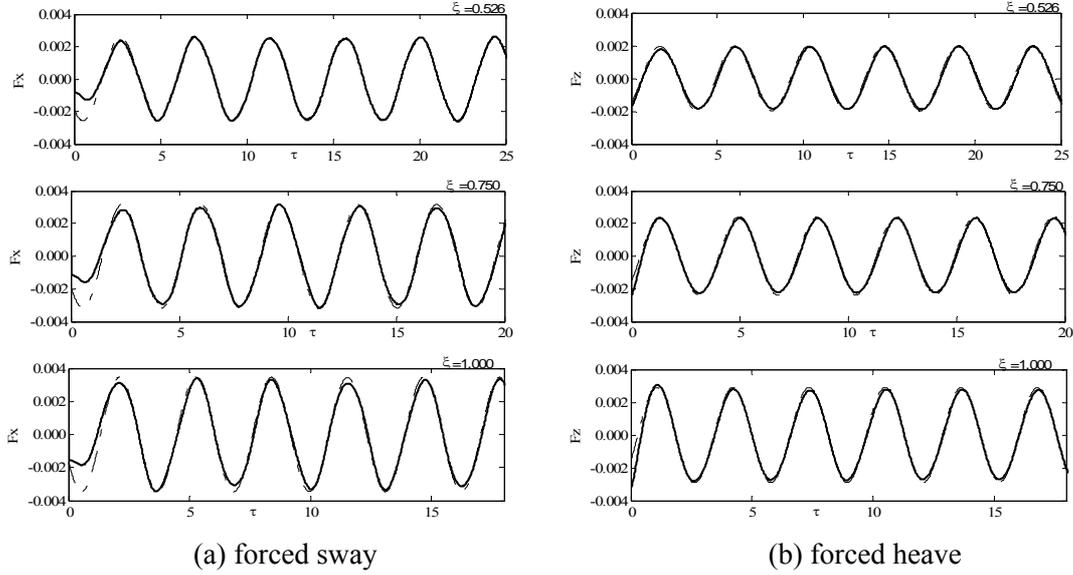
Fig. 5 Comparison of force histories for cases for forced sway/heave with analytical solution
(Solid line: numerical results, Dot line: analytical solution [36])

7.1.1. Comparison with the analytical solution

When the amplitude of the harmonic motion is small, the hydrodynamic force can be evaluated by summing the analytical added mass and radiation damping forces [36], which is used for comparison with numerical results to verify our method. For the numerical simulation, the total tank length is taken as $L \approx 30$ with the length from the wavemaker to the body taken as $L_w \approx 15$ (Fig. 1). The motion amplitude in Eq. (38) are assigned as $a_b = 0.01$. The mesh is unstructured and there are about 35 elements on the free surface in each wave length. The time step is taken as $T/128$, where T is the wave period. The x-direction hydrodynamic force (divided by $\rho g d^2$) in the forced sway and the z-direction hydrodynamic force (also divided by $\rho g d^2$) in the forced heave are plotted in Fig.5 for three cases with different values of ξ, where $\xi = \omega_b^2 \overline{R_b}$ is the frequency parameter. It can be seen that the numerical results agree very well with the analytical ones in all the cases, except in the transient period when the difference is expected because the analytical forces are evaluated for steady state but not for the transient stage. To quantitatively show the accuracy of the numerical results, the relative error (E_r) for the results in Fig. 5 is evaluated by:

$$E_r = \frac{\|f_n - f_a\|}{\|f_a\|} \tag{40}$$

where $\|f\| = \int\limits_{A_e} f^2 dA$; f_n and f_a are the numerical and analytical forces, respectively; and A_e is the

duration over which the error is estimated. Because the accuracy of the forces within the transient period should not be of concern, A_e is taken as the total duration of simulation minus the transient period (about half of wave period). The relative errors evaluated in this way for all the cases in Fig. 5 do not exceed 0.5%.


(a) Sway   (b) Heave
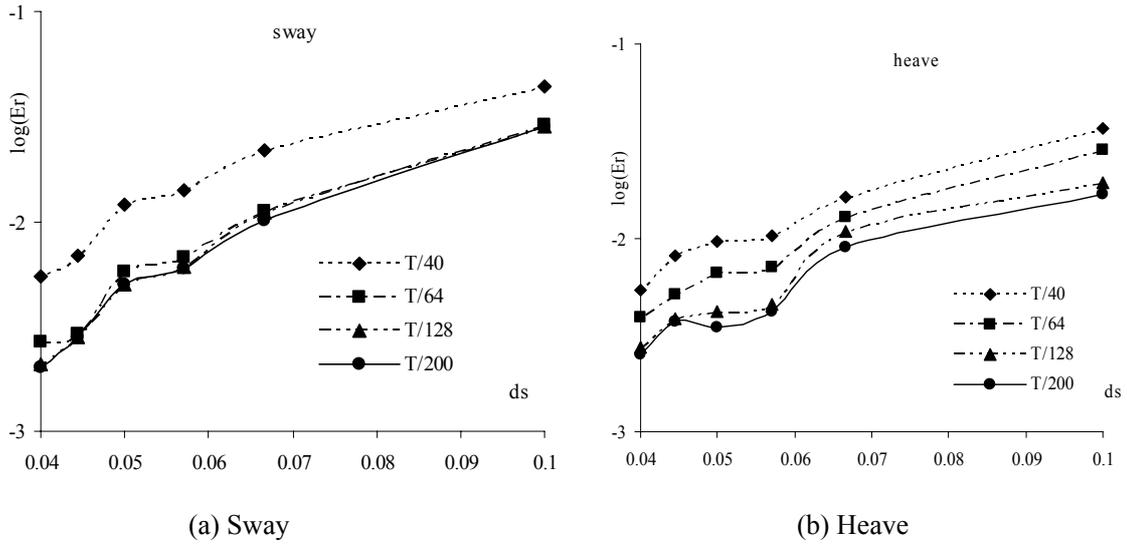
Fig. 6 The relative error for different meshes and different time steps

The characteristics of the relative error are further investigated by considering different time steps and different mesh sizes. For this purpose, the relevant parameters are taken as $a_b = 0.01$ and $\xi = 0.75$ (the corresponding wave length is about $\lambda \approx 2.0$), which are the same as the second case in Fig 5. It should be noted that the investigation on how numerical errors are affected by time steps is relatively easy but not on how they are related to mesh sizes. That is because the errors depend on both mesh sizes and mesh structures and also because it is impractical to consider all possible mesh structures as the unstructured meshes are used in this paper. Apart from these, the mesh sizes constantly change with time for water wave problems. To eliminate the difficulty, a representative mesh size (ds) is used, which is defined as the distance between nodes on the free surface when the water is at rest. The initial mesh structures are almost the same in all cases considered, which feature that the nodes on the free surface, the tank bed and the body surface are uniformly distributed; the distance between nodes on the free surface is roughly twice of that on the body surface and half of that on the tank bed; and the distance between nodes in the vertical direction gradually decrease from the bed to the free surface. The relative errors corresponding to different time steps and different representative sizes (ds) are presented in Fig. 6a and Fig. 6b for sway and heave, respectively. In these figures, the time step is given as the wave period (T) divided by a number. It is observed that the

relative errors are reduced with the decrease in mesh sizes and/or time steps, as expected. Particularly in the ranges of $0 < ds < 0.057$ (about 35 elements in over one wave length) and $0 < dt < T/64$, the relative errors are less than 0.8% for all these cases. This implies that the numerical results with a specified accuracy are achievable by using a sufficiently fine mesh and small time step.

7.1.2. Forced motion with larger amplitudes

In order to investigate the nonlinear effects on waves generated by the forced-motions of the floating body, the cases similar to Fig. 5 but with larger amplitudes are simulated. The wave histories recorded on the left hand side of the body for the case with forced sway (a_b=0.123) is depicted in Fig.7 together with that for a_b=0.0041. Fig.8 shows the wave histories for the forced heave, in which the solid line is the wave history for a_b=0.082, while the dot line is that for a_b=0.0041. In both figures, the wave elevations are divided by the motion amplitude (a_b).
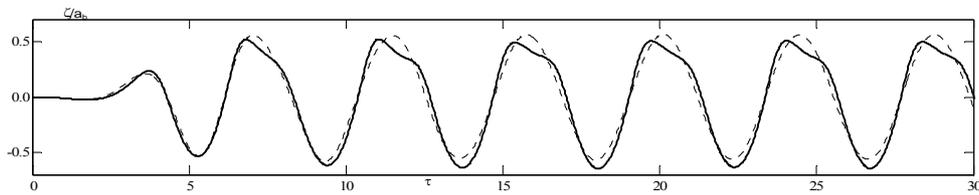

Fig.7 Wave history recorded at *x*=-1 due to forced sway
(L=30, ω_b=1.45, $\xi = 0.75$, solid line: a_b=0.123, dot line: a_b=0.0041)
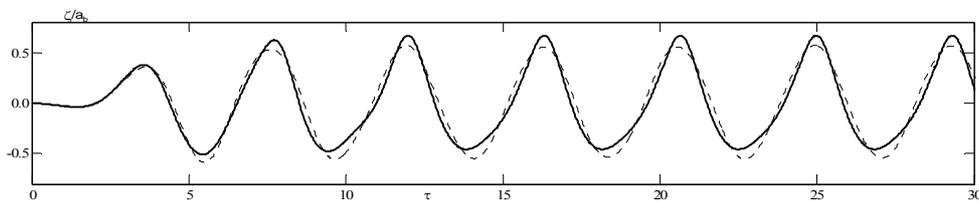
Fig.8 Wave history recorded at *x*=-1 due to forced heave
(L=30, ω_b=1.45, $\xi = 0.75$, solid line: a_b=0.082, dot line: a_b=0.0041)

It can be observed that the wave height seems not to be changed dramatically while the shape of the wave history curve becomes more complicated as the amplitudes of motions becomes larger in the cases for forced sway. In the cases for forced heave, the wave history becomes sharper at crests and flatter at troughs with the increase of the motion amplitudes. All are typical features of nonlinear waves. To show how well the mesh conform to the variation of the body and free surfaces, the mesh configurations for forced sway motions at some time steps are given in Fig. 9. From these figures, it can be seen that the mesh quality near the body surface is maintained even though the motion of the floating body is large. This implies that the suggested method to move nodes works well in the cases including the floating bodies and the free surface.

(a) ≈14.50

(b) ≈15.80

(c) ≈16.66
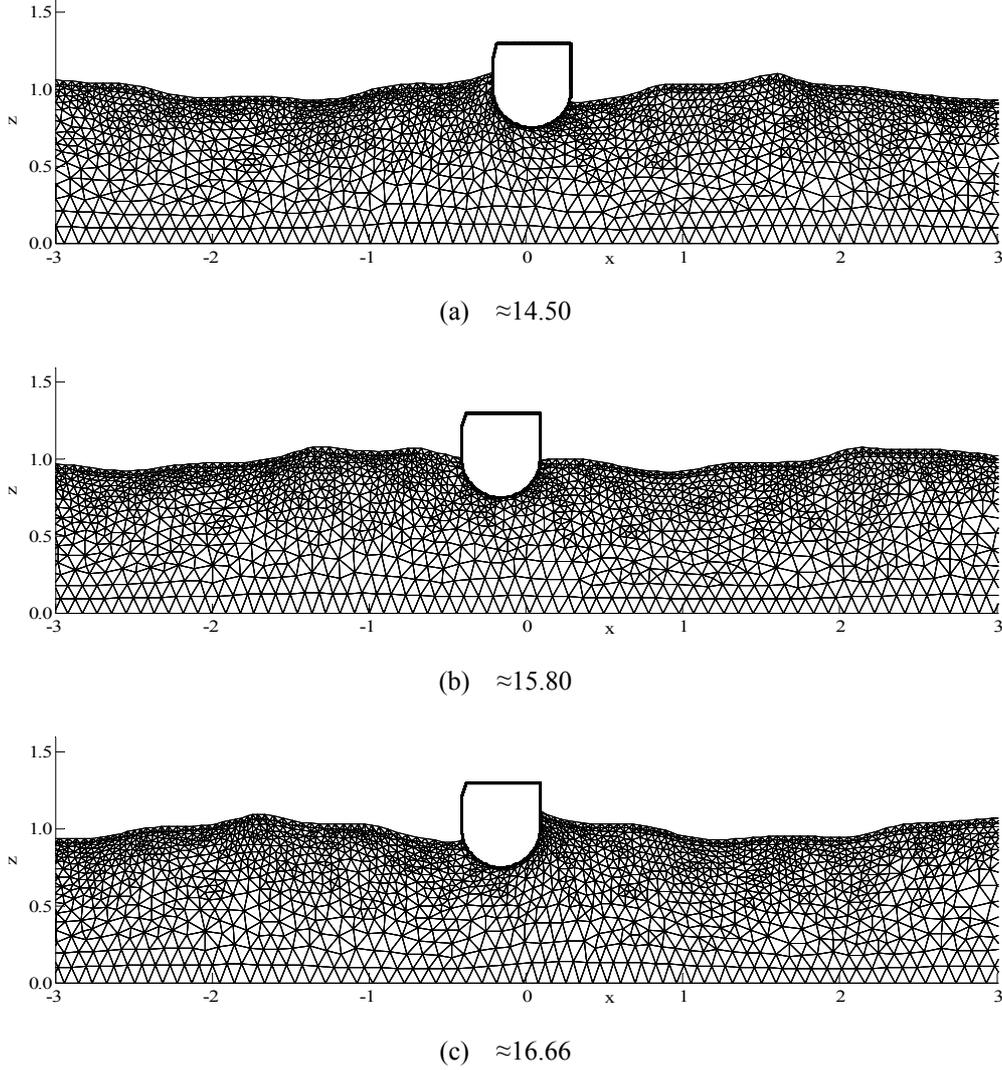
Fig. 9 Mesh configurations for forced sway motion (*L*=30, ω_b=1.45, $\xi = 0.75$ a_b=0.123)

7.2. Free-response floating bodies

After being validated by using cases for forced-motions, the QALE-FEM method is now applied to simulate the motions of a 2D free-response floating body. The incident waves are generated by a wavemaker in a tank and the body is moored to the walls of the tank, as illustrated in Fig. 1. The initial mesh used is similar to Fig 4(b) but the circular cylinder is changed to a barge-type floating body. For this body, the mass is 125kg; the moment of inertia about the gravitational centre is 4.05 kg·m^2; the width (B_b) is 0.5m; the draft is 0.25m; the local radius of round corner of the body is 0.064m and the gravitational centre is located at 0.885m measured from the keel of the barge. In this paper, the mooring line is modelled by a horizontal spring through the gravitational centre with the spring stiffness taken as 197.58 N/m. These parameters and the shape of the body are chosen to be consistent with those in [24] and [37], whose results will be used to validate our numerical ones in Section 7.2.3. In the simulations, the average water depth of the tank is equal to the wave length

determined by $\lambda = \dfrac{2\pi g}{\omega^2}\tanh(2\pi)$. In the following presentation, the frequency (ω) of the wavemaker motion is represented by $\xi = \omega^2 B_b / 2g$; the force is nondimensionalised by using $\rho g d^2$ on the assumption that the length of the 2D body in the direction parallel to the wavemaker is unit; and the roll angle is nondimensionalised by $(\omega_w^2 / g)A_w$, where A_w is the amplitudes of incident waves. Other parameters are nondimensionalised by the same way as in previous sections.

7.2.1 Wavemaker ramp function and artificial damping technique

It is well known that the waves generated by a wavemaker in a tank are characterised by a transient wave profile in the front part of a wave train even though the motion of the wavemaker is purely harmonic. The transient wave profile often consists of several waves with different lengths and heights and a larger wave crest separating the transient and steady parts in the wave train. If one aims to investigate the properties of steady-sate responses, such as RAOs, of floating bodies, the transient waves and corresponding body responses are useless and hence they should be suppressed in order to reduce computational cost. Three methods may be used for this purpose. The first one is to apply wavemaker ramp functions that reduce the wave heights in the transient part. The second is to add artificial viscosity in the dynamic equations of floating bodies (called artificial damping technique), which diminishes the transient body responses. The third method is the combination of the first and the second ones. Details about them are given below.

Two wavemaker ramp functions are investigated, which are similar to those in [32] and [33]. The wavemaker motion corresponding to the first ramp function, called 'Ramp1', is governed by

$$S_w(\tau) = -a\cos(\omega\tau), \tag{41a}$$

$$U_w(\tau) = a\omega\sin(\omega\tau), \tag{41b}$$

$$\dot{U}_w(\tau) = a\omega^2\cos(\omega\tau)(1 - e^{\beta\tau}) \tag{41c}$$

where S_w, U_w and $\dot{U}_w$ are the displacement, velocity and acceleration of the wavemaker respectively; and the coefficient β is the same as that in Eq.(39) with ω_b replaced by ω. In this approach, the generated wave is not modified by the ramp function because the velocity of the wavemaker and so the velocity potential are not affected. The ramping is only performed on the acceleration of the wavemaker, which implies that the value of $\partial\phi/\partial t$ and so forces on bodies are ramped. The wavemaker motion corresponding to the second ramp function, called 'Ramp2', is governed by

$$S_w(\tau) = -a\cos(\omega\tau)r(\tau), \tag{42a}$$

$$U_w(\tau) = \partial S_w / \partial\tau \quad, \tag{42b}$$

$$\dot{U}_w(\tau) = \partial U_w / \partial\tau \tag{42c}$$

$$r(\tau) = \begin{cases} 1 & \tau > T_f \\ \left[1 - \cos(\pi\tau/T_f)\right]/2 & \tau \le T_f \end{cases} \qquad (43)$$

where T_f is the cut-off time of the ramp function and is determined by

$$T_f = \kappa L_w / C_g \qquad (44)$$

in which κ is a coefficient between 0 and 1; and C_g is the group velocity of waves.

The efficiency of Ramp1 and Ramp 2 are investigated with $\xi = 1$, $a = 0.0016$, $L \approx 15$ and L_w ≈ 10. The mesh used is unstructured with about 35 elements on the free surface in each wavelength. For the Ramp2, $\kappa = 0.25$ and $\kappa = 0.5$ are adopted for two cases, respectively.
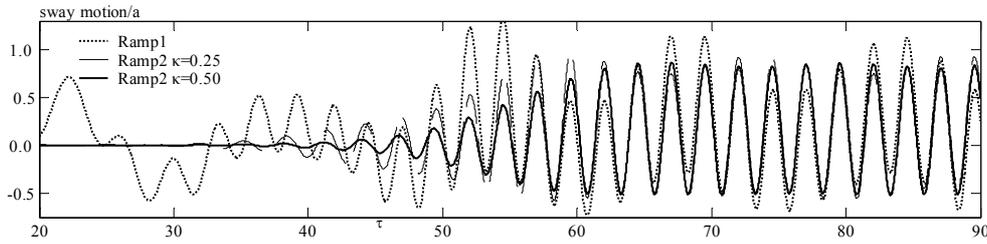
Fig. 10 Sway motion by using different ramp functions

Fig. 10 shows the sway motions obtained by using different ramp functions. It can be observed that Ramp2 can make the calculation become steady sooner than Ramp1, though its effectiveness depends on the value of κ. It should be noted, however, that the waves at the wavemaker generated by using Ramp2 during period $\tau < T_f$ are not the incident waves desired, implying that the waves at the floating body do not become the desired incident waves until $\tau > T_f + L_w / C_g$. In addition, even after the desired incident waves arrive at the floating body, its responses exited by undesired waves do not disappear immediately and so take extra time (T_e) to become those excited by the desired waves. As a result, the time history of motions during the time $\tau < T_f + L_w / C_g + T_e$ should not be considered when estimating RAOs. Based on this analysis, it is obvious that the shorter the sum of $T_f + T_e$, the less CPU time is required for estimating RAOs. As can be seen in Fig. 10, the transient period becomes longer, indicating that T_e becomes larger, with T_f being shorter (i.e., smaller κ) when using the Ramp2 only. Therefore, the reduction in T_f does not necessarily lead to the reduction in the sum of $T_f + T_e$. The other option left to us is to reduce T_e by using the artificial damping technique mentioned above. With this technique, the motion equation, e.g., Eq. (5a), is modified to

$$[M]\dot{U}_c + \beta_a U_c = F \qquad (45)$$

where β_a is the artificial damping coefficient. It is given by

$$\beta_a(\tau) = \begin{cases} 0 & \tau > T_d \\ \alpha\beta_c[1 + \cos(\pi\tau/T_d)]/2 & \tau \le T_d \end{cases} \tag{46}$$

where β_c is the critical damping corresponding to a motion component (such as sway or heave); α is a coefficient; and T_d is the time during which the artificial damping is active. It is found by numerical tests that $T_d = L_w/C_g$ and $\alpha = 0.5$ are appropriate for applications in this paper. Although this technique may be used alone, we will only discuss numerical results obtained by combining it with the Ramp2 to shorten the length of the paper.

To show the effectiveness of the combined method, the two cases for the Ramp2 with $\kappa = 0.25$ and $\kappa = 0.5$ in Fig.10 are considered again but in the first case, both the Ramp2 with $\kappa = 0.25$ and the artificial damping technique with $\alpha = 0.5$ are applied. Fig. 11 gives the results, in which the dashed line denotes the result from the combined method while the solid line represents the result obtained by only using the Ramp2 with $\kappa = 0.5$. It is interesting to see that the response by the combined method using $\kappa = 0.25$ becomes steady at about $\tau = 60$, approximately two wave periods earlier than that by the Ramp2 alone with $\kappa = 0.5$, which is steady at about $\tau = 65$. However, as shown in Fig. 10, the response corresponding to $\kappa = 0.25$ becomes steady much later than that to $\kappa = 0.5$ when using the Ramp2 alone. This indicates that the combined method is more effective to suppress the transient response.
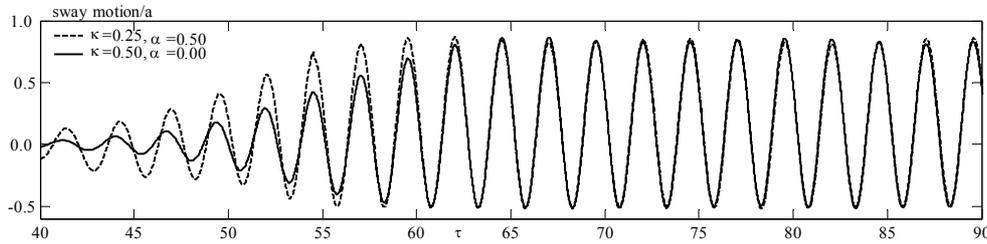

Fig. 11 Sway motion by using artificial damping technique

Apart from these given above, the hydrodynamic forces acting on the body obtained by using different ramp functions and/or the artificial damping technique are also investigated. The results are plotted in Fig.12. It shows that no matter which method is used, the hydrodynamic force acting on floating body tends to the same steady-state limit. This result indirectly indicates that the wavemaker ramp function and artificial damping technique do not affect the RAOs.
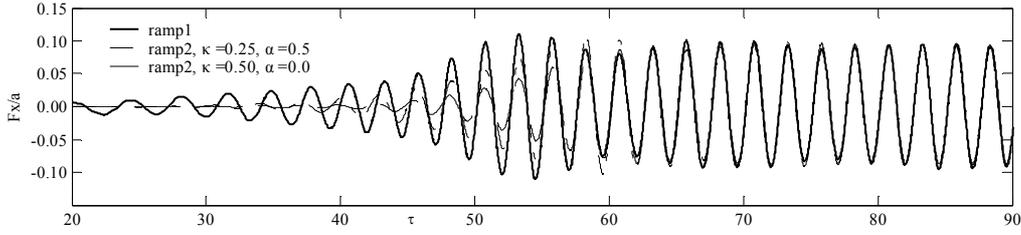
Fig.12 Hydrodynamic force in cases with different ramp functions

### 7.2.2. The convergent properties of the ISITIMFB

One of developments in this paper is the suggestion of the ISITIMFB procedure to find the forces and the motions of the floating body. Its convergent properties, i.e. the iterative counter to achieve a specified accuracy, are presented and discussed in this subsection for the following case: the barge is similar to the one described at the beginning of Section 7.2; the length of the numerical tank is taken as $L \approx 13$ with $L_w \approx 8$; and the dimensionless incident wave height generated is about 0.018 and the frequency parameter is $\xi = 0.4$. Similar to above cases, the mesh used is unstructured with about 35 elements on the free surface in each wavelength. As has been discussed in Section 6, the two most important factors affecting the iterative counter are the time step and the natural period (frequency) of the system. Thus we mainly look at the convergent properties by changing the time step and the natural period in the following.

The results for different time steps are presented by three curves in Fig 13 (a), which correspond to three specified relative errors: 0.1%, 0.5% and 1%. In the figure, there are two rows of numbers under the horizontal axis. The first row represents the number of time steps in each wave period and the second row gives the length of the time step, i.e. the period divided by the number in the first row. In these cases, the mass of the floating body is the same as before, i.e. 125 kg. Under this condition, the value of ξ based on the natural frequency is about $0.5 \sim 0.6$ as shown by the experimental data in [24]. One may observe from this figure that the iterative counter for a specified error decreases with the increase in the number of time steps in each period as expected. One may also observe that the convergence can be achieved within 10 iterations when the control error is 1% and the number of time steps in each period is larger than 64; and that reducing the control errors leads to the increase of iteration but not significantly. It should be noted that the wave frequency is near the natural frequency in these cases. For other cases (not presented) where the wave frequencies are much larger than the natural frequency, the convergent properties are better than those shown here.

The results corresponding to the different natural frequencies at three different control errors are depicted in Fig. 13b, which are obtained by artificially changing the mass in the range of $0.1m_0 \leq m \leq 100m_0$ ($m0$: the mass for Fig. 13a) without changing the mooring stiffness and the shapes of the floating body (i.e., the restoring coefficient being roughly fixed). Under this condition, the square of the natural frequency should be inversely proportional to the mass; and on this basis, the

iterative counter is plotted against the ratio of the mass to m_0 rather than the frequency in the figure. The time step is taken as $T/128$ and all other parameters are the same as those in Fig.13(a). The results in Fig 13b indicate that the iterative counter varies with the change in mass or natural frequency but only in a small range for a large range of change in mass. Similar to Fig. 13a, the difference in the iterative counter does not change dramatically when the control error change from 0.1% to 1%. In addition, the iterative counter is smaller than 10 in the whole range of mass investigated for the control error of 1%.

Another point that needs to be discussed is how the control error in the ISITIMFB procedure affects the computed responses. Fig. 14 shows the comparison of roll motions obtained by using two different control errors for the cases of $\Delta t = T/64$ in Fig. 13. It can be seen that the difference between the results is negligible. Therefore, one may consider the control error of 1% is acceptable in engineering practice but it is recommended that the computed results are compared with those by using a smaller control error such as 0.5%, which is followed when acquiring the numerical results in the paper.
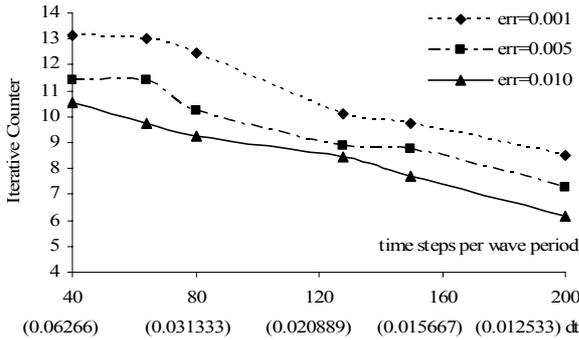
(a) iterative counter *vs* time step
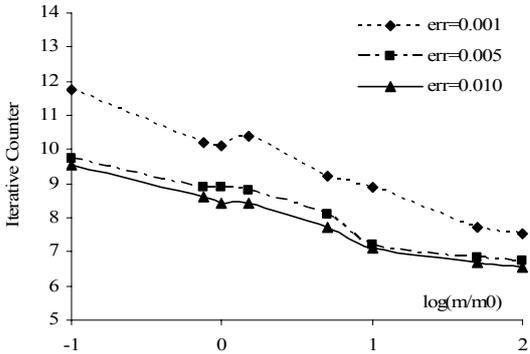
(b) iterative counter *vs* mass

Fig 13 Iterative counters for different time steps and different masses (err: the control iterative error)
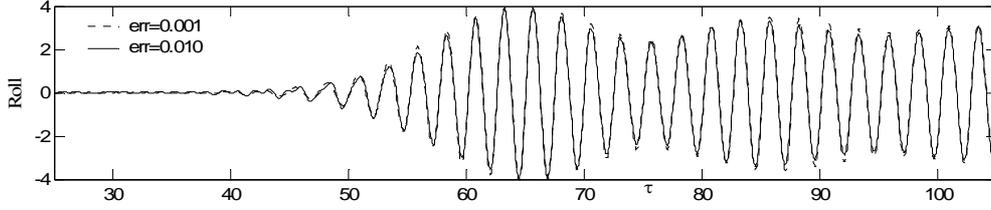
Fig. 14. Comparison of roll histories for different control errors ($dt = T/64$)

### 7.2.3 Comparison with other force calculation methods

In this subsection, the ISITIMFB procedure is firstly compared with a fully explicit method obtained by replacing Eq. (35) with an explicit Adams-Bashforth scheme [35],

$$\vec{U}_b^{n(k)} = \vec{U}_b^{n-1} + \frac{\Delta t}{2}(3\vec{A}_b^{n-1} - \vec{A}_b^{n-2}) .$$

For the fully explicit method, the iteration is not needed. The time step is taken as $T/200$ and $T/64$; and other parameters are the same as those used in Fig.14. The results are plotted in Fig. 15. From Fig. 15(a), it is observed that the ISITIMFB leads to similar results to the fully explicit integration procedure when the time step is small ($T/200$). However, when the time step becomes larger ($T/64$), the results from the ISITIMFB have negligible difference from those for smaller time steps while the results from the fully explicit integration procedure poses evident disagreement with those using smaller time step (Fig.15(b)). This indicates that the ISITIMFB proposed in this paper can give more accurate results at the same time step or can use larger time steps for specified accuracy and so needs less CPU time for a given period of simulation than the explicit method.
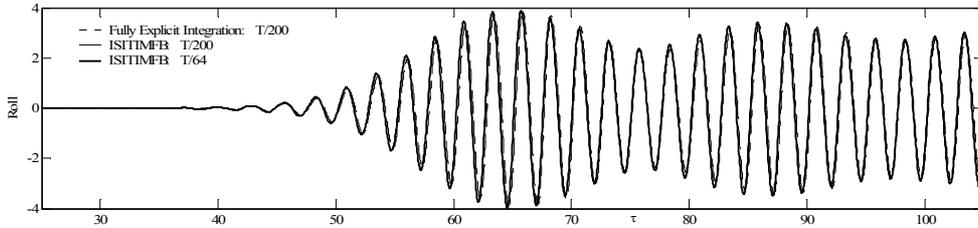
(a)
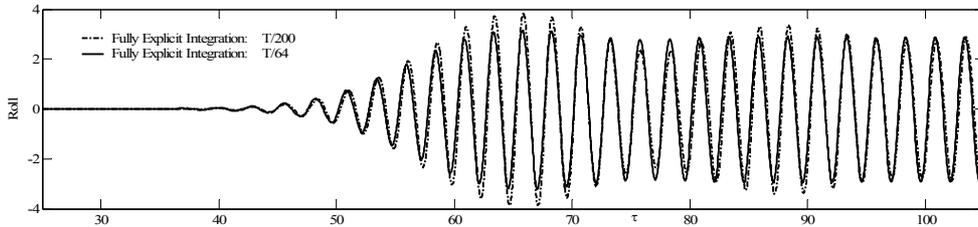
(b)

Fig.15 Comparison of roll motions from the ISITIMFB and explicit procedures

To further demonstrate the behaviours of the ISITIMFB, its results are then compared with those

from fully-updated and frozen-coefficient 4th-order Runge-Kutta schemes ([23]) and shown Fig. 16, using the same parameters except for the wave height and the time step as for Fig. 15. To consider the same case as in [23], the dimensionless incident wave height of 0.0025 and the time step $\Delta t = T / 40$ are used here. As can be seen, the presented procedure leads to steady-state results that agree well with those from the full-updated Runge-Kutta method while the frozen-coefficient Runge-Kutta scheme does not give similar results even when the time step is as small as $T/128$. The results for the frozen-coefficient Runge-Kutta scheme also tends to be unstable as indicated in [23]. This clearly demonstrates that the ISITIMFB can alleviate the instability problem of the frozen-coefficient method and can be as accurate and robust as the full-updated Runge-Kutta method but without the need of multiple updating of fluid domain geometries and so of the coefficient matrix in one time step forward.
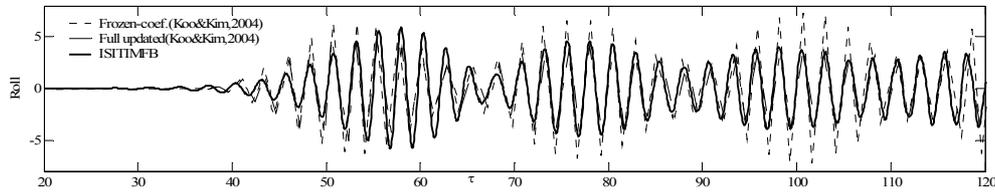

Fig.16 Comparison of roll motions from ISITIMFB and other methods
(Frozen-coefficient scheme: $\Delta t = T / 128$; ISITIMFB and Fully updated Runge-Kutta method: $\Delta t = T / 40$)

7.2.4. RAOs of sway, heave and roll motions

To further validate the QALE-FEM method in the cases with a floating body, the RAOs of sway, heave and roll motions of the barge are compared with the linear solution by using frequency domain analysis as given in [24] and the experimental data in [37]. In the numerical simulations, Ramp2 together with the artificial damping technique is employed, for which the associated parameters are taken as $\kappa = 0.25$, $T_d = L_w / C_g$ and $\alpha = 0.5$; as in above sections, the unstructured mesh is adopted with about 30 elements on the free surface in each wavelength and the time step is taken as $\Delta t = T / 128$. For all cases considered here, the amplitudes of the wavemaker are adjusted properly so that generated incident wave heights are either 0.01m or 0.07m, which are the same as those in the cited publications.

The RAOs of sway, heave and roll motions corresponding to different incident waves are plotted in Fig. 17 together with the results from other publications. They are estimated by performing the FFT analysis on the steady-state portion of the time histories of corresponding motions. As can been seen, the present numerical results are closer to the linear solution when the incident waves are small (0.01m) but closer to the experimental data when the wave height becomes larger (0.07m). This is reasonable because the experimental data for the larger wave height contain nonlinear effects that are taken into account by the nonlinear numerical simulations but not by the linear solution.
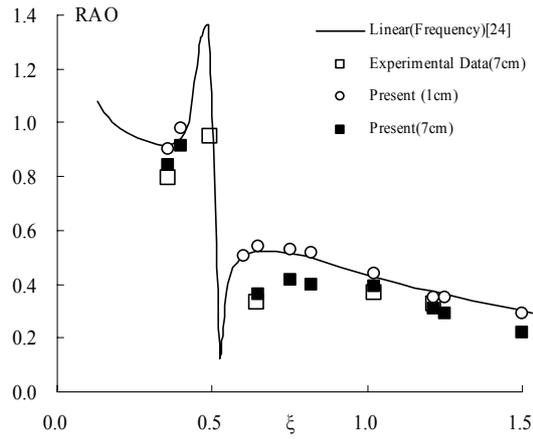
(a) RAO of sway motion
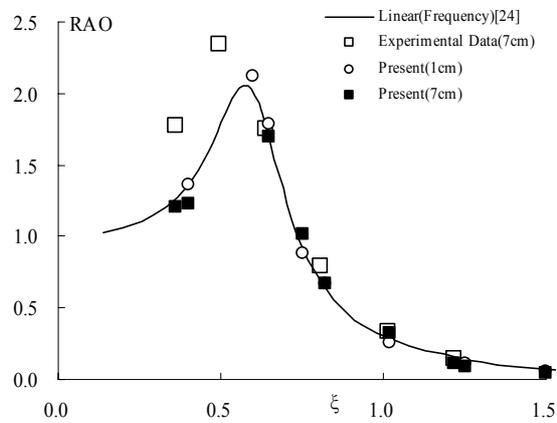
(b) RAO of heave motion
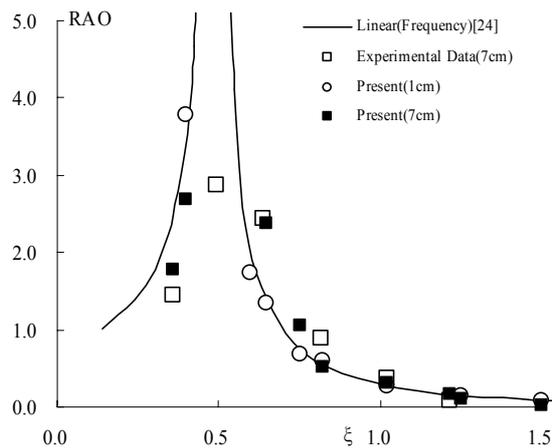
(c) RAO of roll motion

Fig.17 RAOs of sway, heave and roll as a function of ξ

However, the difference between experimental data and numerical results is obvious in the area

near resonance frequencies. That may be due to the fact that the viscosity is not considered in numerical simulations whereas it is inevitable in experiments. To demonstrate that the conjecture might be true, an empirical damping force is added into the roll equation, which is formed by a damping coefficient multiplying the roll velocity. The value of the damping coefficient is taken as 1.5% or 2.8% of the critical damping coefficient in two different simulations. It should be noted that the empirical damping added here plays different rules and is for different purposes from the artificial damping discussed above. The empirical damping here is applied from the start to the end of simulations to approximately model the real viscosity and so affects the amplitudes and RAOs even after the motions become steady. The artificial damping discussed in Section 7.2.1 is applied in a specified simulation period from the start in order to suppress the transient responses and does not affect the amplitudes and RAOs after motions become steady.

The RAOs of the roll motion near the resonant frequency obtained by using different empirical damping for the same cases in Fig. 17 are shown in Fig.18 together also with the linear solution and the experiment data. It can be seen that when the empirical roll damping is 2.8% of the critical damping, our numerical results agree quite well with the experimental data in the resonant area in this case. Based on this, one may envisage that with an appropriate empirical roll damping, our numerical method can give good approximate results even when the viscosity plays an import rule.
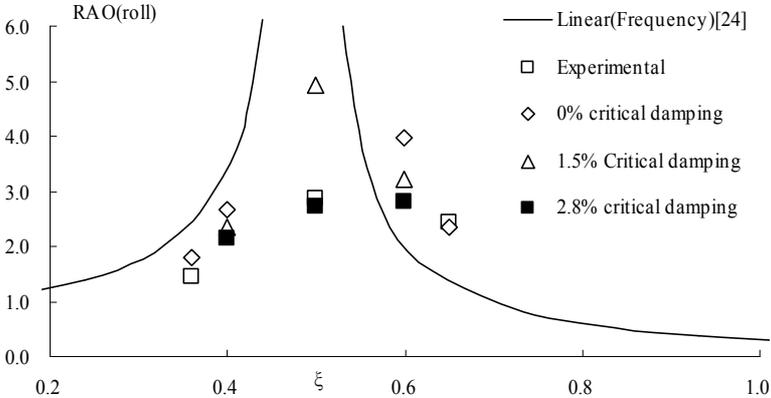

Fig. 18. RAO of roll motion in case with roll artificial damping

The cases in Figs. 17 and 18 are also simulated by using different meshes, different iterative control errors and different time steps. Some results are shown in Fig. 19, from which one can see that the difference between them is invisible. This signifies that the numerical errors due to selecting different mesh sizes, time steps and iterative control errors are negligible for the results in these two figures.
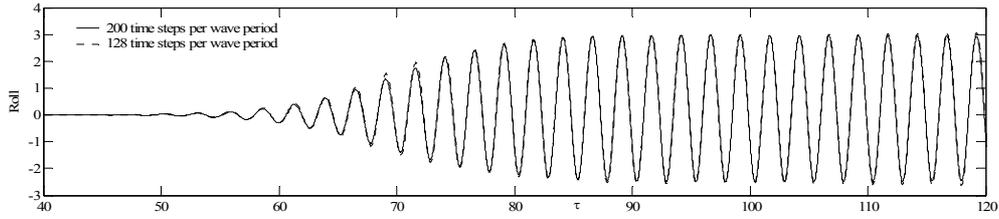
(a) different time steps(iterative control error is taken as 0.005,30 nodes per wave length)
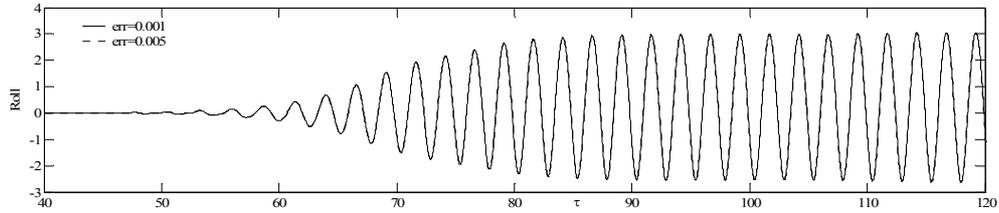
(b) different iterative control errors($\Delta t = T/128$,30 nodes per wave length)
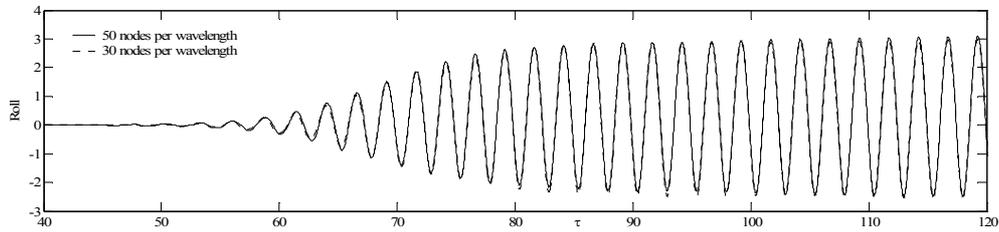
(c) different meshes($\Delta t = T/128$,iterative control error is taken as 0.005)

Fig.19. Roll motion in terms of different time steps, iterative control error and meshes
($\xi = 0.5$, the wave height is 0.07m)

7.2.4. Transient responses of floating bodies

So far, discussions about responses of floating bodies to waves have been focused on the RAOs and how to calculate them in a more efficient way. In this section, some results are presented for transient responses of floating bodies, which are also used to show the nature of nonlinear interaction between floating bodies and waves. For the cases considered in this section, the tank length is $L \approx 10$ with $L_w \approx 5$ and the frequency parameter is $\xi = 0.65$ that is near the resonant value as seen in Fig. 17. The generated wave heights are about 7cm. Because we are interested here in the transient behaviours here, the ramp function is not applied.

The wave elevations and body responses are shown in Fig.20, which illustrates how the body responds to the transient waves. One may see that the body motion, particularly the roll angle in this case, is dramatically larger when the front part of the wave trains just reaches the body than those in other instances and so larger than those predicted by using RAOs. It is clearer in Fig. 21, where the roll time history is plotted. This implies that the transient responses rather than RAOs should be considered in design in order to check if a floating body is safe when it is subjected to a transient waves.

(a) τ≈18.17

(b) τ≈25.07

(c) τ≈34.47

(d) τ≈35.72

(e) τ≈51.39

(f) τ≈52.64
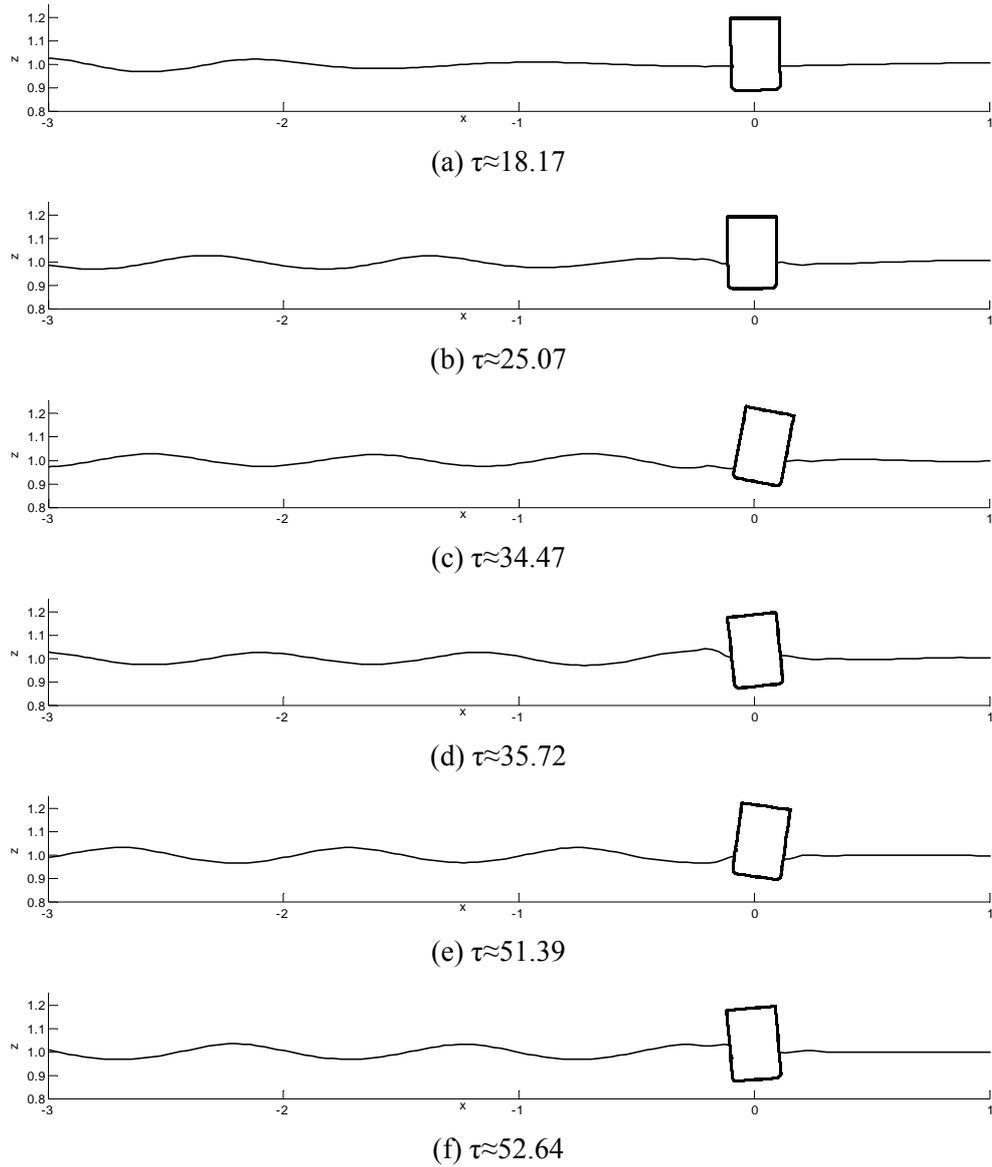
Fig. 20 wave elevation and body motion ($\xi = 0.65$, the wave height is about 7cm)
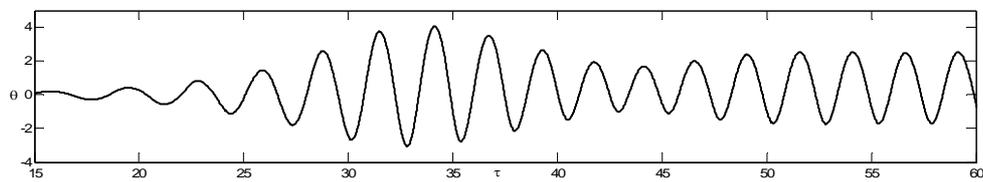
Fig.21 time history of roll for the wave height of 7cm and $\xi = 0.65$

　　To show the nonlinear effects in this case, the sway force and roll moment acting on the floating body is plotted Fig.22. It can be observed that all the curves are quite complex. For the sway force, the curve in one wave period is not symmetric about the apex point in that period. For the roll moment, the curve exhibits the sharper high crests and flatter and shallower troughs. All are features

of nonlinearity.

(a) sway force

(c) roll moment
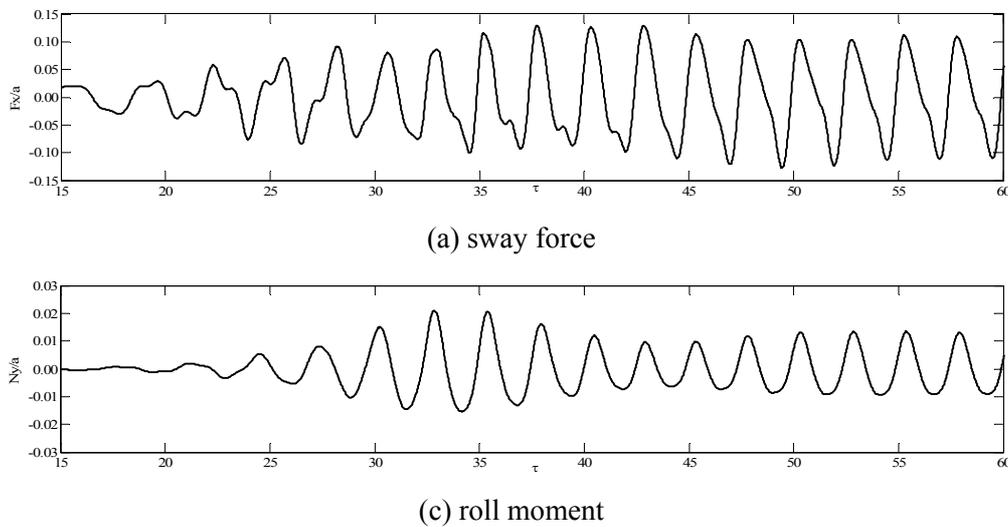
Fig.22 Force and moment acting on the floating body ($\xi = 6.5$, the wave height is about 7cm)

8. Computational efficiency of QALE-FEM for cases with free-response floating bodies

The significant development of the QALE-FEM is that the unstructured mesh is moved to conform to the motion of boundaries. As indicated in [1], without floating bodies, the mesh quality can be kept well. With the inclusion of floating bodes, their motions, particularly large angular motions, can make the mesh near body surfaces undergo large variations and so it is necessary to check if the methodology for moving meshes in the QALRE-FEM could also produce good quality of meshes in these cases. Some illustrations have been given for the cases with forced motions in Fig. 9. Apart from these, extensive investigations have also been made for the cases associated with free - response floating bodies during the development of the method. One case will be presented in this section to demonstrate the effectiveness of the method in producing good meshes at all time steps. The same floating body described in Section 7.2 is used, which is subjected to a wave with the height of 7cm and the frequency parameter of $\xi = 0.65$ in a tank of *L*=10. This case is run on a PC (Pentium 2.53GHz processor, 1G RAM). The fluid domain is discretised into about 129,732 elements and 28,725 nodes.

Fig. 23 presents the mesh at different instances, where the right column illustrates the enlarged mesh in the vicinity of the body surface. Fig. 23a depicts the initial unstructured mesh while Fig. 23b and Fig. 23c show the meshes in the same area but after quite long time simulation. These figures demonstrate that the original refinement and distribution are maintained well and all elements are in satisfactory shape during the simulation. In addition, negative elements, which are of concern when using the linear spring analogy method, do not appear. Nevertheless, certain changes in the sizes and shapes of individual elements are observed and expected because the fluid domain varies with

propagation of waves. It is these changes that make it possible to conform to the moving boundaries at all time steps and so to achieve satisfactory results as demonstrated in previous sections. In addition, the CPU time spent on moving the mesh at each time step is on average about 1s, including 0.01s for moving mesh on the body surface, approximately the same as the CPU time spent on sandbar problems in [1]. The CPU time spent on all calculations in one step is about 7s on average. It indicates that the method used to move mesh in the QALE-FEM in cases with floating bodies is as efficient as in cases without floating bodies. It also indicates that useful results for a problem like these may be obtained in several hours by using a normal PC.

(a) Initial mesh (τ=0.0)

(b) $\tau\approx39.6$

(c) $\tau\approx43.11$
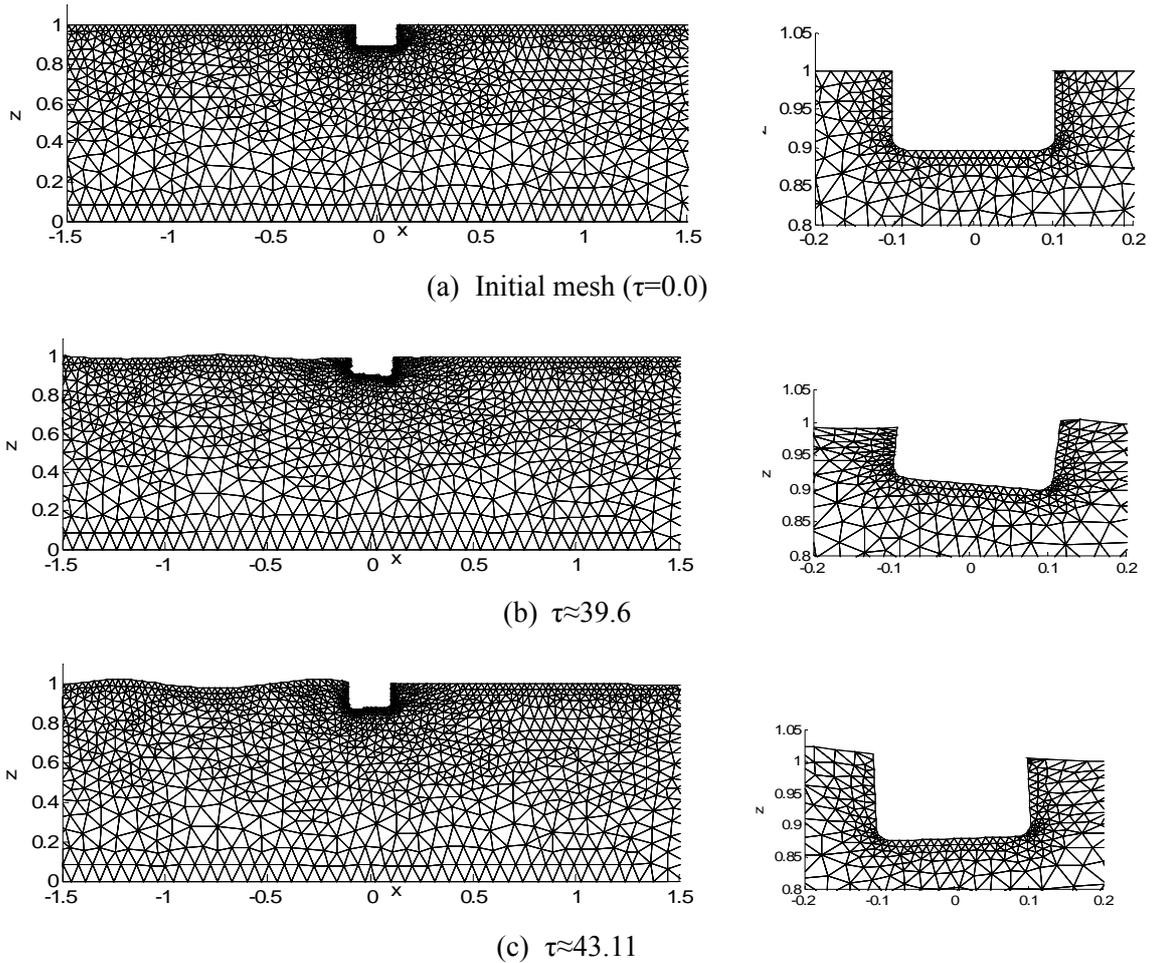
Fig. 23 Mesh at different instances (Left: mesh around body; Right: enlarged mesh)

For cases with floating bodies, the ISITIMFB procedure for calculating forces has been developed in this paper. The accuracy and stability of the procedure have been investigated in Section 7.2.2. In this section, the efficiency of the procedure is discussed by comparing it with mode-decomposition method with the 4th-order Runge-Kutta method as the time integration scheme. In the later method, the motion is decomposed into 4 modes in 2D cases to find the solution for the potential derivatives ($\partial\phi/\partial t$) by solving 4 different boundary value problems in addition to one for the velocity potential (ϕ). Thus, total 5 different boundary value problems must be dealt with for one

sub-step and therefore total 20 different boundary value problems for calculating ϕ and $\partial\phi/\partial t$ need to be solved in one time step forward. In addition, updating of the coefficient matrix is necessary to achieve stable solution as discussed in Section 7.2.2. On the other hand, when using our ISITIMFB, the number of iterations in one step forward is on average 7 for the case in Fig. 23 by using the control error of 1% in the procedure and so about 15 boundary value problems need to be solved without the necessity of updating the coefficient matrix. Therefore, for this case, the CPU time required by the ISITIMFB is less than 75% of that required by the mode-decomposition method. Although the CPU time used by the ISITIMFB is problem-dependent, it is more efficient as long as the number of iterations in the ISITIMFB is less than 10; this may not be exceeded in many cases unless choosing a control error and a time step that are unnecessary small, as indicated in Section 7.2.2. In addition, if the mode-decomposition method with the 4th-order Runge-Kutta scheme is used in our QALE-FEM method, the calculation of velocities on the free surface with unstructured meshes must be performed five times in one time step forward, which likely requires considerable more CPU time. Consequently, the ISITIMFB is a procedure that is efficient and is best matched with our QALE-FEM method.

8. Conclusion

In this paper, the QALE-FEM developed in our previous papers [1] and [2] is extended to simulate nonlinear interaction between water waves and 2D floating bodies based on the FNPT Model. In this method, the boundary value problems for the velocity potential and its time derivatives are solved by using a finite element method; and the mesh is moved in order to conform to the variations of the free surface and the body surface by the spring analogy method specially proposed for these problems. The method allows the efficient use of unstructured mesh without the need to regenerate it at every time step, which is a necessary and very costly feature of the conventional FEM. The main developments in this paper are the techniques required for dealing with 2D nonlinear wave-body interactions. They include a scheme for moving mesh near and on the body surface, the ISITIMFB procedure for efficiently estimating the velocities and accelerations of bodies as well as the forces on them, the method for evaluating the fluid velocity on the surface of bodies and the use of wavemaker ramp functions and an artificial damping technique for shortening the transient period.

The newly extended method has been validated by comparing its numerical predictions of forces on bodies undergoing forced motions with analytical solutions. Comparison has also been made between the numerical results from this method for the RAOs of a free-response floating body and experimental data. Good agreement has been achieved in all the comparisons. Assessments are made on the efficiency of moving mesh and the quality of elements obtained by the QALE-FEM. These show that the unstructured mesh quality is satisfactorily maintained at all time steps even when the complex interactions between waves and free-response floating bodies are involved and also that the QALE-FEM requires a little time for moving mesh. Due to these developments, the useful results for a 2D floating body may be obtained in several hours using a normal PC.

9. Acknowledgement

10. Reference

[1] Ma, Q.W., Yan, S., Quasi ALE finite element method for nonlinear water waves. J. Comput. Phys, in press (2005).

[2] Yan S., Ma Q.W., Application of QALE-FEM to the interaction between nonlinear water waves and periodic bars on the bottom. 20th international workshop on water waves and floating bodies, Norway, 2005.

[3] Lachaume, C., Biausser, B., Grilli, S. T., Fraunie, P., Guignard, S., Modeling of Breaking and Post-breaking Waves on Slopes by Coupling of BEM and VOF Methods, Proceedings of the International Offshore and Polar Engineering Conference, 2003, 1698-1704.

[4] Clauss G.F., Steinhagen U., Numerical simulation of nonlinear transient waves and its validation by laboratory data, Proceedings of the 9th International Offshore and Polar Engineering Conference, Brest, France, 1999, 368-375.

[5] Ma, Q.W., Wu, G.X., Eatock Taylor, R., Finite element simulation of fully non-linear interaction between vertical cylinders and steep waves. Part 1: Methodology and numerical procedure, Int.J.Numer. Meth. Fluids,36(2001) 265-285.

[6] Ma, Q.W., Wu, G.X., Eatock Taylor, R., Finite element simulation of fully non-linear interaction between vertical cylinders and steep waves. Part 2: Numerical results and validation, Int.J.Numer. Meth. Fluids, 36(2001) 287-308.

[7] Longuet-Higgins, M.S., Cokelet, E.D., The deformation of steep waves on water: I. a numerical method of computation, Proc. R. Soc. Lond. A 350 (1976) 1–26.

[8] Vinje, T. & Brevig, P., Nonlinear ship motion. In Proc. 3rd Int. Conf. on Numerical Ship Hydrodynamics, Paris, France, (1981) 257–268.

[9] Lin, W. M., Newman, J. N. & Yue, D. K. Nonlinear forced motion of floating bodies. In Proc. 15th Symp. on Naval Hydrology, Hamburg, Germany, 1984, 33–49.

[10] Wang, P., Yao, Y., Tulin, M., An efficient numerical tank for nonlinear water waves, based on the multi-subdomain approach with BEM, Int. J. Num. Meth. Fluids, 20(1995) 1315-1336.

[11] Kashiwagi, M., Full-nonlinear simulations of hydrodynamic forces on a heaving two-dimensional body. J. Soc. Nav. Archit. Jpn. 180(1996) 373–381.

[12] Cao, Y., Schultz, W.W. & Beck, R.F., Three-dimensional desingularised boundary integral method for potential problems, Int. J. Num. Meth. Fluids, 12(1991) 785-803.

[13] Celebi, M.S., Kim, M.H., Beck, R.F., Fully nonlinear 3D numerical wave tank simulation, J. Ship

Res. 42 (1998) 33–45.

[14] Grilli, S.T., Guyenne, P., Dias, F., A fully nonlinear model for three-dimensional overturning waves over arbitrary bottom, Intl J. Numer. Meth. Fluids, 35(2001) 829-867.

[15] Kim M.H., Celebi M.S., Kim D.J., Fully nonlinear interactions of waves with a three-dimensional body in uniform currents. Applied Ocean Research, 20 (1998) 309–321

[16] Wu, G.X., Eatock Taylor, R., Finite element analysis of two dimensional non-linear transient water waves, Appl. Ocean Res. 16(1994) 363–372.

[17] Wu, G.X., Eatock Taylor, R., Time stepping solution of the two dimensional non-linear wave radiation problem, Ocean Eng. 22(1995) 785–798.

[18] Ma, Q.W., Numerical simulation of nonlinear interaction between structures and steep waves, PhD Thesis, Department of Mechanical Engineering, University College London, UK, 1998.

[19] Cao Y., Beck R. F. & Schultz W. W., Nonlinear Computation of Wave Loads and Motions of Floating bodies in Incident Waves. 9th international workshop on water waves and floating bodies, Kuju, Oita, Japan, 1994, 33-37

[20] Tanizawa, K. A nonlinear simulation method of 3-D body motions in waves (1st Report). J. Soc. Nav. Arch. Japan, 178(1995) 179-191

[21] Tanizawa K., Minami M. On the accuracy of NWT for radiation and diffraction problem. The 6th Symposium on Nonlinear and Free-Surface Flow, 1998.

[22] Tanizawa K, Minami M. & Naito S., Estimation of wave drift force by numerical wave tank. Proc. 9th ISOPE Conf. vol3, Brest, 1999

[23] Koo W., Fully nonlinear wave-body interactions by a 2D potential numerical wave tank. PhD Thesis, Texas A&M University, 2003.

[24] Koo W., Kim M., Freely floating body simulation by a 2D fully nonlinear numerical wave tank. Ocean Engineering, 31(2004) 2011-2046.

[25] Kashiwagi, M., Momoda, T., Inada, M., A time-domain nonlinear simulation method for wave-induced motions of a floating body. J. Soc. Nav. Archit. Jpn. 84(1998) 143–152.

[26] Kashiwagi M., Nonlinear simulations of wave-induced motions of a floating body by means of the mixed Eulerian-Lagrangian method, Mech. Engrs,214(2000) 841-855

[27] Wu, G.X., Hu, Z.Z., Simulation of nonlinear interactions between waves and floating bodies through a finite-element-based numerical tank, Proceedings A of the Royal Society, 460 (2004), No. 2050, 3037-3058.

[28] Ma Q. W., Patel M. H., On the nonlinear forces acting on a floating spar platform in ocean waves. Applied Ocean Research, 23(2001) 29-40

[29] Sen, D Numerical simulation of motions of two-dimensional floating bodies. J. Ship Research 37, 4 (1993) 307-330.

[30] Dalen, E.F.G, Numerical and theoretical studies on water waves and floating bodies. PhD thesis, University of Twente, Enschede, 1993

[31] Tanizawa K., The state of the art on numerical wave tank. 4th Osaka colloquium on seakeeping performance of ships, Osaka, Japan, 2000, 95-114

[32] Eatock Taylor, R, Wang, B.T., Wu, G.X., On the transient analysis of the wavemaker, 9th International Workshop on Water Waves and Floating Bodies, Kuju, Oita, Japan, 1994.

[33] Eatock. Taylor R., Wave-maker ramp functions in numerical tanks. 20th international workshop on water waves and floating bodies, Norway, 2005.

[34] Whittle. P. Prediction and regulation by Linear Least-Square Methods. London: The English Universities Press Ltd.,(1963).

[35]William Gear C. Numerical Initial Value Problems in Ordinary Differential Equations. Prentice-Hall , Inc. Englewood Cliffs, New Jersey.(1971),102-115.

[36] Faltinsen O.M., Sea loads on ships and offshore structures. Cambridge University press, Unite Kingdom, 1990.

[37] Nojiri N., Murayama K., A study on the drift force on two dimensional floating body in regular waves. Trans. West-Japan Soc. Nav. Arch, Vol.51 (1975).

CITY City University London

The University for business

and the professions

Dr. Qingwei Ma
Senior Lecturer in Fluids Engineering
School of Engineering and Mathematical Sciences
City University
Northampton Square, London EC1V 0HB, UK
Tel. (+44) 020 7040 8159
Fax. (+44) 020 7040 8566
E-mail: q.ma@city.ac.uk
12th May 2006

Numerical simulation of fully nonlinear interaction between steep waves and 2D floating bodies using the QALE-FEM method

Manuscript Ref: JCOMP-D-05-00722

Dear Editor,

The enclosed are the revised version of the above paper. The main changes based on the referees' comments and suggestions are summarised as below:

1) The last paragraph at the end of Section 4.2 is rewritten to clarify the method for treating bodies with sharp corners.
2) Two more paragraphs are added in Section 6 to present more details and discussions about the iterative procedure.
3) One new figure and paragraph are added in Section 7.1.1 to give more details about convergent studies.
4) A new subsection (7.2.2) is added to present the discussion and results for the investigations on the properties of the ISITIMFB procedure, which includes two new figures (Figs. 13 and 14)
5) Fig. 14 and Fig. 15 are replaced by Fig. 17 and Fig. 18, respectively. In the new figures, the values of RAOs at the same frequencies as experiments are added and some unnecessary results from other publications are removed following the suggestions of one of the referees. In addition, Fig. 19 and corresponding discussions are added to convince people that the difference of the numerical results from the experimental ones at the resonant frequency is due to the ignorance of viscosity in the potential model.

The detailed responses to the referee's comments are given on separate pages enclosed with this letter. Some minor changes made in this version are also mentioned at proper places on those pages.

Yours sincerely

Qingwei Ma

Manuscript Ref: JCOMP-D-05-00722

Responses to the comment of Reviewer #1

The authors appreciate very much the reviewer's constructive comments. The followings are our replies (Italic fonts) to reviewer's questions.

This manuscript describes extensions to the QALE-FEM method (developed by the authors and others) to treat nonlinear wave interaction with freely floating bodies in 2D. The extensions include: An improved method for dynamic re-griding near the moving body; an improved scheme for computing fluid velocities on the body; and a semi-implicit method for treating the coupled body and fluid dynamics. The model is validated using linear forced motion of a semi-circle, and calculations are presented for the nonlinear motions of a moored barge-like structure in waves. The motion RAOs are compared to experimental results, linear theory, and other calculations. The claim is made that the current calculations are closer to the linear theory results at small wave amplitude and closer to the experimental results at large amplitude. It is also argued that the difference between the computed and experimental results can be explained by viscous damping. Neither of these claims is convincingly supported by the results shown.

The work described by this paper is however interesting and worth publishing after a moderate-to-major revision of the manuscript addressing the deficiencies itemized below and detailed in the attached marked up copy.

We have modified the text following the most suggestions given in the marked copy by the reviewer.

1. Convergence and order of accuracy of the method: The validation test case presented (one is discretisation compared to the exact result leading to the vague statement that errors are less than 0.5%) does not give any indication of the convergence properties of the model, nor does it say anything about the overall order of accuracy of the model. Detailed convergence and accuracy studies also appear to be lacking from previous publications regarding this model but if they exist they should be referred to. Can it be demonstrated that the model converges to the exact linear solution as the grid is refined? If so, what is the rate of convergence? These questions need to be answered.

The overall order of the numerical scheme is determined by the shape functions NJ in (19) (among other things) and the manuscript does not mention what these functions are chosen to be. We can guess, based on previous publications, that they are bi-linear polynomials. Does this lead to first-order or second-order accuracy? What is expected, and can this be verified numerically?

We agree with the reviewer that the convergent issues should be addressed. Actually, all results in our previous publications related to the FEM method and in the first version of this paper are carefully validated by comparing with other known results and/or by using different meshes and time steps, though they may not be presented in the format as the reviewer kindly suggested. In the revised versions, two figures (Fig 6 a & b) are included and one paragraph is added to give the details about the convergent studies in the way the reviewer suggested.

As for the statement related to the error less than 0.5% in our original version, we would like to point out that the specific value of the error was obtained for the cases in Fig. 5 as mentioned in the first version of the manuscript but not for other cases.

It is our mistake to fail to mention that the shape function is linear, which is rectified in the revised version. The results in the added figure (Fig. 6 a & b) demonstrate that the accuracy is indeed the first order, as expected.

There are also some more basic properties of the model which seem not to have been illuminated by previous publications. Without a structure in the domain, how well does the model predict the propagation of linear and nonlinear waves? Consider a periodic domain, where both linear and fully nonlinear analytic solutions exist (e.g [Fenton(1988)]). How many elements per wavelength are required to achieve a certain level of accuracy per

period of propagation? Can the model handle highly nonlinear waves? I.e. how close to the stable breaking limit can the model successfully propagate waves?

In our previous publications, we think we have made sufficient investigations for all presented cases without a structure, which include the comparison of numerical results with the linear solution for progressive waves made by a wavemaker (Ma, Wu And Eatock Taylor, 2001, Part 2, and Ma & Yan 2006); with experimental data from three different laboratories (Ma, Wu And Eatock Taylor, 2001, Part 2 and Ma & Yan 2006) for steep waves; and with the linear and second order analytical solutions of sloshing waves (Ma, Wu And Eatock Taylor, 2001, Part 2 and Ma, and Wu, "Second order transient waves around a vertical cylinder in a tank", Journal of Hydrodynamics, Vol.7,1995, No.4, pp72-81). In addition, our results are also compared by other researchers with their results, for examples, Kim ("Numerical simulation of sloshing flows with impact load", Applied Ocean Research, Vol. 23, 2001, pp. 53-62) for a case with a nearly-breaking sloshing wave. Although some of these investigations were carried out by using our conventional FEM, the comparisons between results for waves without a structure obtained by using the QALE-FEM and our conventional FEM in Ref [1] showed very good agreement. One this basis, it seems to us that the behaviors of the model and method have been well validated for the cases without structures. Of course, the model and the method would become more convincing if they would have been validated against more results obtained by other experiments and other numerical methods including one in Fenton (1988). Nevertheless, because this paper is mainly concerned with problems associated with floating structures, we wish the reviewer would agree that we would not go into more details about problems without structures on the basis that more details about the convergent properties are added in the revised version.

As for how many elements per wavelength are required to achieve a certain level of accuracy, one may see this from the new Fig. 6 a & b.

2. A new semi-implicit scheme is presented for solving the coupled problem of the wave and body dynamics and important details of how this scheme is derived are missing, as noted directly in the manuscript.

More details are given in this version. In addition, a new subsection (7.2.2 in this version) is added, in which the convergent properties of the ISITIMFB procedure are discussed in more details.

3. §7.2.2: In figures 14 & 15 the motion RAO's of a barge are compared to experiments and other calculations. On the basis of these results, two conclusions are made: 1) The calculations are close to linear theory for small amplitude waves and closer to experiments for larger amplitude waves; 2) The difference between the nonlinear calculations and the experiments can be explained by viscous damping effects. The results in those figures do not convincingly support these conclusions for several reasons.

These conclusions are supported now by more convincing discussions, thanks to the reviewer's suggestions. The details are given below corresponding to the reviewer specific comments.

(a) The plots are too small to read properly, especially with so much data on them. I suggest larger plots and removal of the calculations by Koo & Kim and Tanizawa which simply provide distraction.

We have removed the results of Koo & Kim and Tanizawa, which makes our results clearer.

(b) The experimental and the calculated data points are not at the same frequencies which make it impossible to properly compare them. The calculations need to include all the same frequencies as the experiments, and ideally many more.

In the previous version of the manuscript, our numerical results are compared to the numerical results from Koo & Kim and Tanizawa at the same frequencies, which are not at the same frequencies as the experimental data. In the revised one, the results of Koo & Kim and Tanizawa are removed following the suggestion of the reviewer as mentioned above and the results at almost the same frequencies as the

experiments are added in Fig 17 (that replaces Fig. 14 of the old version), except at the resonant frequency which is discussed below in answering question (c). In addition, some results at other frequencies, at which experimental data are unavailable, are also included. These results for the cases presented agree well with the linear results when the wave amplitude is relative smaller and with the experimental data when the wave amplitude (almost the same as that in the experiments) is larger, as would be seen.

(c) Given the lack of any kind of demonstration of convergence of the calculations, the claim that the difference between experiment and calculation can be attributed to viscous damping is suspect. The results shown in figure 15 are in any case quite ambiguous. Some indication that these are converged results is required, the data points need to line up (in terms of frequency), and all the data points need to be discernable.

In addition to the discussions about the convergent properties of the ISITIMFB procedure added in Section 7.2.2 and of the overall method in Section 7.1.1, the response of the floating body at the resonant frequency presented in Fig. 18 (replacing Fig 15 of old version) are also simulated by using different meshes, time steps and control errors for the ISITIMFB and the corresponding time histories are plotted in Fig. 19. Good agreement between all the results may sufficiently support our second conclusion.

Manuscript Ref: JCOMP-D-05-00722

Responses to the comment of Reviewer #2

The authors appreciate very much the reviewer's constructive comments. The followings are our replies (Italic fonts) to reviewer's questions.

Recommendation
In my opinion, the paper requires moderate to major revisions to render it acceptable for publication. The paper quite obviously is a sequel to Ref. [1] of the manuscript. The extension pertains to the introduction of a floating body. There are significant textual overlaps with [1]. Nevertheless, the new developments warrant separate publication, provided that they are presented in a consolidated form. Below, I provide comments to support my recommendation and to assist the authors in revising the manuscript.

> *As the reviewer pointed out, this is a sequel to Ref [1] and so there are some overlaps in the introduction and in Sections 2 and 3. The author thinks that they are necessary to give readers sufficient background about the new developments presented in this paper.*

Major comments
1. My main objection against the paper is that some parts of the extension to floating bodies have not matured sufficiently. In particular, the node-movement scheme on the body is still rather crude, as acknowledged by the authors in §4.2. I would recommend the authors to consolidate the new aspects of their method before publishing it. That is, the authors should propose a mature scheme for the node movement on the body.

> *These might be due to our misleading discussions to justify the method for moving nodes on body surface with sharp corners at the end of Section 4.2 of the previous manuscript, which is now rectified. It should be noted that all numerical methods for the potential model have difficulties with dealing with the sharp corners. One way to overcome them is to smooth the corner, which is also tested in our work. In addition to this, we also suggest another technique - prescribing a node at the corner. Both of them work well and give consistently converged results, as demonstrated by the new discussions in Section 7.2.2 and 7.2.4 . We think the method for moving nodes on the body surface become sufficiently matured to be published, though peoples may continuously suggest other techniques to deal with sharp corners as in other numerical methods.*

2. As the iterative scheme for computing forces and velocities at the floating body in §6 is considered an important new contribution, the authors should specify how this iterative method is different from previous iterative methods, e.g., Ref. [19] of the manuscript.

> *To make it clearer, the second paragraph from the end of Section 6 is added.*

3. Moreover, the iterative scheme for computing forces and velocities at the floating body is inadequately tested in the numerical experiments. Of course, the convergence of this iterative procedure is of pivotal importance. Conjecturally, the convergence of this procedure deteriorates with increasing time step and decreasing mass of the floating body. The authors should also provide a systematic study of the convergence of their iterative procedure (error v.s. iteration counter) at various sizes of the time step and floating-body masses.

> *One new section (7.2.2) is added to discuss the convergent properties of the iterative scheme associated with time steps and floating-body masses, together with the convergent studies with respect to the mesh sizes added in Section 7.1.1.*

4. Furthermore, I recommend that the authors request a native English speaker to check the paper for spelling and grammar. In its present form, certain parts of the paper are difficult to read.
   A native English speaker has kindly checked the spelling and grammar.

1

Minor comments

1. The statement of the kinematic condition (2) is rather strange. Normally, the kinematic condition is given by

$$\frac{\partial \zeta}{\partial t} + \frac{\partial \Phi}{\partial x}\frac{\partial \zeta}{\partial x} + \frac{\partial \Phi}{\partial y}\frac{\partial \zeta}{\partial y} - \frac{\partial \Phi}{\partial z} = 0. \qquad (1)$$

The authors should specify the relation between (2) and the above conventional form of the kinematic condition.

   There are two formulations for the free surface boundary conditions: one is based on the Eulerian view and the other on the Lagrangian view. The one given by the reviewer is based on the Eulerian view. The one we use is based on the Lagrangian view, which was first suggested by Longuet-Higgins and Cokelet ("The deformation of steep surface waves on water: I. A numerical method of computation." Proceedings of the Royal Society of London A 1976; 350: 1–26) and has been employed by many researchers who model fully nonlinear water waves. But there were some errors in Eq. (2) of the previous manuscript, which is now rectified.

2. What is the connotation of Dx/dt in (2)? This notation is at the least unconventional and must be defined. Moreover, the $D\phi / Dt$ in (3) should be $\partial\phi / \partial t$
   This is now rectified

3. I have reservation against the terminology QALE method. In principle, the method is just an ordinary ALE method. The Q derives from the property that the mesh motion does not appear in the equations in the form of temporal derivatives. This, however, is a result of the fact that Laplace's equation is independent of time. Hence, the Q is a result of the underlying equation, and not of the method.

   The QALE-FEM features not only that the mesh motion does not affect the governing equations including the free surface and body boundary conditions depending on temporal derivatives but also that (1) the mesh is moved by a distinctive technique combing the spring analogy method and self-adaptive principle suggested for the free surface problems by the authors; (2) the fluid velocity is estimated by a method developed for the continuously moving mesh and (3) the coupling of the floating body with the nonlinear waves is dealt with by the ISITIMFB procedure, best matching with the QALE-FEM method. These features distinguish it from the conventional FEM and also the ordinary ALE.

4. The authors should specify how the boundary conditions are incorporated into the finite-element formulation in §2.4. The treatment of BCs is of critical relevance, especially in free-surface flow applications.

   We agree with the reviewer that the treatment of BCs is of critical relevance. We think it has been sufficiently discussed in our previous publications. One paragraph is added at the starting of the section 2.4 to give specific references. We wish the reviewer would agree that fully repeating them would lead to more overlaps and would distract readers' attention away from our focus of this paper.